

# Ferromagnetism and Transport in the Double-Exchange Model, with and without Phonons; Application to the Manganites

D M Edwards and A C M Green

Department of Mathematics, Imperial College, London SW7 2BZ, UK

November 6, 2018

## Abstract

An introduction is given to the many-body coherent potential approximation (CPA) for the double-exchange (DE) model and the Holstein-DE model, the latter including coupling of the electrons to local phonons as well as to the local spins. It is shown how the method can treat the local spins and phonons quantum-mechanically and how it is equivalent to dynamical mean field theory in the classical limit. In the Holstein-DE model a full discussion is given of the cross-over from weak electron-phonon coupling through intermediate coupling, where small-polaron bands begin to appear, to strong coupling where some results similar to those of standard small-polaron theory are recovered. The theory is applied to ferromagnetic manganites with a full discussion of magnetic, transport, and spectroscopic data. It is found that many manganites are in the critical regime on the verge of small-polaron formation, which explains their sensitivity to parameters such as applied magnetic field and pressure.

## Contents

<b>1</b>	<b>Introduction</b>	<b>2</b>
<b>2</b>	<b>CPA for the Hubbard model</b>	<b>3</b>
<b>3</b>	<b>The many-body CPA for the DE model</b>	<b>5</b>
<b>4</b>	<b>Resistivity in the paramagnetic state of the DE model</b>	<b>8</b>
<b>5</b>	<b>Magnetism in the DE model</b>	<b>9</b>
<b>6</b>	<b>Many-body CPA for the Holstein-DE model</b>	<b>11</b>
<b>7</b>	<b>Application to manganites</b>	<b>16</b>
<b>8</b>	<b>Conclusion</b>	<b>24</b>

# 1 Introduction

Magnetic materials exhibiting metallic behaviour can often be considered as systems of local moments coupled to electrons in a conduction band by local exchange interactions. The Hamiltonian for such a system is

$$H_{\text{DE}} = \sum_{ij\sigma} t_{ij} c_{i\sigma}^\dagger c_{j\sigma} - J \sum_i \mathbf{S}_i \cdot \boldsymbol{\sigma}_i - h \sum_i (S_i^z + \sigma_i^z), \quad (1)$$

where  $c_{i\sigma}^\dagger$  creates an electron of spin  $\sigma$  on lattice site  $i$ ,  $\mathbf{S}_i$  is a local spin operator and  $\boldsymbol{\sigma}_i = (\sigma_i^x, \sigma_i^y, \sigma_i^z)$  is a conduction electron spin operator defined by

$$\sigma_i^+ = \sigma_i^x + i\sigma_i^y = c_{i\uparrow}^\dagger c_{i\downarrow}, \quad \sigma_i^- = \sigma_i^x - i\sigma_i^y = c_{i\downarrow}^\dagger c_{i\uparrow}, \quad \sigma_i^z = \frac{1}{2} (n_{i\uparrow} - n_{i\downarrow}) \quad (2)$$

with  $n_{i\sigma} = c_{i\sigma}^\dagger c_{i\sigma}$ . The three terms of equation (1) describe hopping of the conduction electrons, exchange coupling between local and itinerant spins and coupling to an external magnetic field. If the local exchange coupling arises from hybridization between the localized and itinerant electrons, as in anomalous rare earth systems exhibiting heavy fermion behaviour, the exchange parameter  $J$  is negative. The Hamiltonian (1) is then often called the Kondo lattice model in view of its connection with the Kondo impurity model which has a local spin on one site only [1]. When Hund's rule coupling is dominant  $J > 0$  and the system is sometimes called a ferromagnetic Kondo lattice. This is misleading since for  $J > 0$  there is no connection with the Kondo effect.

For  $J > 0$  it is useful to distinguish two distinct physical regimes, depending on the magnitude of  $J$  compared with the width  $2W$  of the conduction band. If  $J \ll W$ , as in a normal rare earth metal, the exchange coupling can be treated as a perturbation which gives rise to the Ruderman-Kittel-Kasuya-Yosida (RKKY) interaction between local moments. In most rare earth metals this interaction, which oscillates in space, leads to oscillatory or spiral configurations of the localized  $f$  electron moments. The uniform ferromagnet Gd is an exception. In this weak coupling regime the Hamiltonian (1) is usually referred to as the  $s - f$  or  $s - d$  model.

If  $J \gg W$  the exchange coupling can no longer be treated as a perturbation. A conduction electron can only hop onto a site with its spin parallel to the local moment at that site. Furthermore if the number of conduction electrons per atom  $n \leq 1$  double occupation of a site is strongly suppressed. A single electron at a site, with its spin parallel to the local spin  $\mathbf{S}$ , enjoys an exchange energy  $-JS/2$  which is lost if a second electron hops on. The system is therefore a *strongly correlated electron system*, just like the Hubbard model in the regime of strong on-site Coulomb interaction  $U$ , and for  $n = 1$  the system is a Mott insulator. In much of the theoretical work on the present model the local spins are treated as classical vectors, corresponding to  $S \rightarrow \infty$ . Since for  $J \gg W$  the itinerant spin must always be parallel to the local spin on each site, the effective hopping integral for hopping between sites  $i$  and  $j$  becomes  $t_{ij} \cos(\theta_{ij}/2)$ , where  $\theta_{ij}$  is the angle between the classical spins  $\mathbf{S}_i, \mathbf{S}_j$ . The cosine factor arises from the scalar product of two spin 1/2 eigenstates with different axes of quantization. The resultant band narrowing in the paramagnetic state favours ferromagnetism in order to lower the kinetic energy. This mechanism for ferromagnetism was first introduced by Zener [2] and developed by others [3, 4, 5]. Since it involves strong exchange coupling on two adjacent atoms it is known as double-exchange. Consequently the Hamiltonian (1) in the strong-coupling regime  $J \gg W$  is called the double-exchange (DE) model. This paper is concerned with the DE model, with quantum and classical local spins, and with its extension to include coupling of the electrons to local phonons. We call this extended model the Holstein-DE model.

The paper provides a simple introduction to the many-body coherent potential approximation (CPA) described in detail in our previous papers [6, 7, 8, 9] and reviews the results. When spins and phonons are treated classically the CPA is equivalent to the dynamical mean field theory (DMFT) approach of Furukawa [10, 11] and Millis et al. [12]. A fully quantum mechanical treatment within DMFT is a difficult numerical task which has not yet been done. The many-body CPA may be regarded as a useful analytic approximation to DMFT which becomes exact in the classical limit.

The main application we have in mind is to the manganites  $\text{La}_{1-x}\text{D}_x\text{MnO}_3$ , where D is a divalent ion such as Ca or Sr. Recently there has been renewed interest in these systems due to the discovery of colossal magnetoresistance (CMR), the name given to a large reduction in resistivity in an applied magnetic field [13]. For  $x = 0$ ,  $\text{LaMnO}_3$  is an antiferromagnetic insulator, but on doping with  $0.2 < x < 0.5$ , the system becomes a ferromagnetic metal. The CMR phenomenon is observed in the vicinity of the Curie temperature  $T_C$ . In applying equation (1) to these systems the local spins  $\mathbf{S}_i$  are of magnitude  $S = 3/2$ , corresponding to three localized Mn d electrons of  $t_{2g}$  symmetry, and the band is derived from Mn d states of  $e_g$  symmetry. The band contains  $n = 1 - x$  itinerant electrons per atom. Since we are interested in doped ferromagnetic systems, the antiferromagnetic interaction between neighbouring local spins plays no important role and is neglected. A more serious simplification is the use of a single s band, instead of two d bands based on orbitals of  $e_g$  symmetry. We discuss this in section 7.

In section 2 we introduce the many-body CPA by means of the Hubbard model and in section 3 we develop it for the more complicated case of the DE model with quantum local spins. In section 4 we discuss the electrical resistivity of the paramagnetic state in the DE model and show, as first stressed by Millis et al. [14], that the DE model is unable to describe the physics of the manganites completely. In section 5 we briefly discuss the variation of  $T_C$  as a function of band-filling  $n$ . The development of the many-body CPA for the Holstein-DE model is discussed in section 6 and a comparison with standard small-polaron theory is made in the limit of strong electron-phonon coupling. For intermediate coupling we discuss the crossover, with increasing temperature, from polaronic behaviour to a situation where the phonons behave classically, the case considered by Millis et al. [12]. In section 7 we consider the application of the Holstein-DE model to the manganites. Comparison with experimental data leads to the conclusion that typical manganites lie in the critical intermediate coupling regime which is not fully described by previous theories. We summarise briefly in section 8.

## 2 CPA for the Hubbard model

To introduce the many-body CPA we consider the Hubbard model, which is a simpler model for strongly correlated electrons than the DE model with quantum spins. The Hamiltonian for this model is

$$H_{\text{H}} = \sum_{ij\sigma} t_{ij} c_{i\sigma}^\dagger c_{j\sigma} + U \sum_i n_{i\uparrow} n_{i\downarrow} \quad (3)$$

and Hubbard [15] set out to find an approximation to the one-electron retarded Green function  $G_{\mathbf{k}\sigma}(\epsilon)$  which is exact in the atomic limit  $t_{ij} = 0$ . He used the equation of motion method and the idea of the alloy analogy described below. It turns out that Hubbard's approach, without the minor "resonance broadening correction", is equivalent to the CPA which was developed later [16]. The CPA derivation of Hubbard's result is much simpler than the original equation of motion method. However we had to resort to an extension of the original method to derive the many-body CPA for the DE model, with and without phonons, in the general form needed to discuss magnetic properties. In this paper we restrict the derivation to the paramagnetic state in zero magnetic field, although we summarize some more general results.

The alloy analogy consists in considering the  $\uparrow$ -spin electrons, say, to move in the potential due to static  $\downarrow$ -spin electrons, frozen in a random configuration which must be averaged over. Thus a one-electron Hamiltonian for  $\uparrow$ -spin is obtained from (3) by taking the last term to be  $U \sum_i n_{i\uparrow} \langle n_{i\downarrow} \rangle$  where  $\langle n_{i\downarrow} \rangle$  takes the value 1 with probability  $n_\downarrow$  and 0 with probability  $1 - n_\downarrow$ . Here  $n_\sigma$  is the number of  $\sigma$ -spin electrons per atom. It is important to note that the alloy analogy is quite distinct from the Hartree-Fock approximation in which  $\langle n_{i\sigma} \rangle = n_\sigma$  for all  $i$ . In the alloy analogy a  $\sigma$ -spin electron moves in a random potential given by  $U$  on  $n_\sigma$  sites and 0 on  $1 - n_\sigma$  sites. In the CPA the random potential is replaced by a uniform, but energy-dependent, effective potential  $\Sigma_\sigma(\epsilon)$  for an "effective medium". This effective potential, in general complex, is called the coherent potential and is in fact the electron self-energy. The procedure for determining  $\Sigma_\sigma$

is to insist on a zero average t-matrix for scattering by a central atom, with potential  $U$  or 0, set in the effective medium. Equivalently the average of the site-diagonal element  $G_\sigma(\epsilon)$  of the Green function, for each type of central atom, is put equal to the site-diagonal element of the Green function for the effective medium. Thus

$$G_\sigma = n_{\bar{\sigma}} \frac{G_\sigma}{1 - (U - \Sigma_\sigma) G_\sigma} + (1 - n_{\bar{\sigma}}) \frac{G_\sigma}{1 + \Sigma_\sigma G_\sigma} \quad (4)$$

and

$$G_\sigma(\epsilon) = \frac{1}{N} \sum_{\mathbf{k}} \frac{1}{\epsilon - \epsilon_{\mathbf{k}} - \Sigma_\sigma(\epsilon)} = G_0(\epsilon - \Sigma_\sigma(\epsilon)) \quad (5)$$

where the bare band Green function is given by

$$G_0(\epsilon) = \int d\epsilon' \frac{N_0(\epsilon')}{\epsilon - \epsilon'} \quad (6)$$

Here  $\epsilon_{\mathbf{k}} = \sum_j t_{ij} \exp[i\mathbf{k} \cdot (\mathbf{R}_i - \mathbf{R}_j)]$  is the band energy, where  $\mathbf{R}_i$  is the position of site  $i$ ,  $N_0(\epsilon)$  is the corresponding density of states per atom and  $N$  is the number of lattice sites. Equations (4) and (5) are to be solved self-consistently for  $\Sigma_\sigma(\epsilon)$  and hence for the local Green function  $G_\sigma(\epsilon)$ . Equation (4) may be written as

$$G_\sigma = \frac{n_{\bar{\sigma}}}{\Sigma_\sigma + G_\sigma^{-1} - U} + \frac{1 - n_{\bar{\sigma}}}{\Sigma_\sigma + G_\sigma^{-1}} \quad (7)$$

This may be compared with the exact Green function for the atomic limit ( $t_{ij} = 0$ ) which is given by [15]

$$G_\sigma^{\text{AL}}(\epsilon) = \frac{n_{\bar{\sigma}}}{\epsilon - U} + \frac{1 - n_{\bar{\sigma}}}{\epsilon} \quad (8)$$

where in this retarded Green function  $\epsilon$  has a small positive imaginary part. Hence

$$G_\sigma(\epsilon) = G_\sigma^{\text{AL}}(\Sigma_\sigma + G_\sigma^{-1}) \quad (9)$$

Clearly this CPA equation is exact in the atomic limit, when  $N_0(\epsilon) = \delta(\epsilon)$  and it follows from equation (5) that  $\Sigma_\sigma + G_\sigma^{-1} = \epsilon$ . Solution of the CPA equation becomes simple if the density of states  $N_0(\epsilon)$  is taken to be of the elliptic form

$$N_0(\epsilon) = \frac{2}{\pi W^2} (W^2 - \epsilon^2)^{1/2} \quad (10)$$

where  $2W$  is the bandwidth. Then from equation (6)

$$G_0(\epsilon) = \frac{2}{W^2} \left[ \epsilon - (\epsilon^2 - W^2)^{1/2} \right] \quad (11)$$

Introducing this expression for  $G_\sigma$  in equation (5), and solving for  $\epsilon - \Sigma_\sigma(\epsilon)$ , we find

$$\Sigma_\sigma + G_\sigma^{-1} = \epsilon - W^2 G_\sigma / 4 \quad (12)$$

Hence equations (8) and (9) give an algebraic equation for  $G_\sigma$ .

Solving this type of equation for  $G_\sigma$ , Hubbard [15] calculated the density of states  $N_\sigma(\epsilon) = -\pi^{-1} \text{Im} G_\sigma(\epsilon)$ , considering particularly the paramagnetic state  $n_\uparrow = n_\downarrow = n/2$  and concentrating on the half-filled band case  $n = 1$ . He showed that for  $U/W$  greater than a critical value, equal to 1 in the present approximation, a gap opens in  $N(\epsilon)$  at the Fermi level so that the system becomes an insulator as envisaged by Mott. For  $U \gg W$  the density of states consists of two peaks centred on  $\epsilon = 0$  and  $\epsilon = U$ , these being broadened versions of the  $\delta$ -functions at these energies in the

atomic limit. Furthermore, for general band-filling  $n$ , the spectral weights in the two peaks are the same as in the atomic limit.

The CPA for the Hubbard model has some serious defects. There are no self-consistent solutions with magnetic order. Furthermore in the paramagnetic metallic state, for  $n < 1$  or for  $n = 1$  with  $U/W$  less than the critical value, the system is never a Fermi liquid. There is never a sharp Fermi surface at  $T = 0$  with a Migdal discontinuity in the Bloch state occupation number, as pointed out by Edwards and Hewson [17]. This is due to the absence of states with infinite lifetime at the Fermi level, since within the alloy analogy all states are scattered by disorder. A modification of the CPA to remedy this defect, retaining the analytic simplicity of the method, had some limited success [18, 19, 20]. However the most satisfactory approach is DMFT which involves numerical solution of an associated self-consistent impurity problem [21, 22]. DMFT may be regarded as the best local approximation, in which the self-energy is a function of energy only, and is exact in infinite dimension.

The many-body CPA is considerably more satisfactory for the DE model than it is for the Hubbard model, as discussed in the next session. There is one limit, the case of classical spins ( $S = \infty$ ), in which the CPA is identical to DMFT. This is because classical spins are static and an alloy analogy of frozen disordered spins is completely justified. DMFT for the DE model has only been implemented for classical spins [10, 11] and the many-body CPA discussed in the next section provides an approximate analytic extension of DMFT to quantum spins. The system orders ferromagnetically below a Curie temperature  $T_C$ , as it should, and the disordered spin state above  $T_C$  should be well described. However, the accuracy of the ground state at  $T = 0$  for finite  $S$  is unclear. The saturated state with all itinerant and local spins completely aligned, which is the ground state for  $S = \infty$  (we are always considering large  $J$  in the DE model), is never a self-consistent CPA solution for finite  $S$  [6]. Actually the parameter range of stability of the saturated ground state is unknown. It has been shown rigorously that for  $J = \infty$  it is unstable for  $S = 1/2$  and  $0.12 < n < 0.45$ , with a simple cubic nearest-neighbour tight-binding band [23]. If the true ground state is not saturated it seems unlikely to be a uniform (spatially homogeneous) ferromagnet, with partially ordered local and itinerant spins, as in the uniform CPA ground state for finite  $S$ . Such a state would probably not be a Fermi liquid, just as in CPA, unless the electrons making up the spin  $S$  became partially delocalised with spectral weight at the Fermi level. Such speculation goes beyond the DE model.

### 3 The many-body CPA for the DE model

In an earlier paper [6] we developed the many-body CPA for the DE model using an extension of Hubbard's equation of motion method. Hubbard's "scattering correction" becomes more complicated owing to the form of the interaction term in the DE model whereby electrons can flip their spin via exchange of angular momentum with the local spins. This dynamical effect couples the equations for  $G_{\uparrow}$  and  $G_{\downarrow}$  and was first treated by Kubo [24] in a one-electron dynamical CPA. The main feature of our many-body CPA is that we recover Kubo's one-electron CPA as  $n \rightarrow 0$  and the correct atomic limit for general band-filling  $n$  as  $t_{ij} \rightarrow 0$ . In a second paper [7] we showed the equivalence to DMFT in the limit  $S \rightarrow \infty$ ,  $J \rightarrow \infty$ . The full equation of motion derivation of the many-body CPA is required to obtain general results in the presence of a magnetic field and/or magnetic order [7]. However it turns out that in the zero-field paramagnetic state we can deduce the CPA equation from the atomic limit Green function  $G_{\sigma}^{\text{AL}}$  and equation (9), just as in the Hubbard model. We shall therefore not repeat the full derivation in this paper although we shall discuss results on magnetic properties in section 5.

The atomic limit Green function,  $G_{\uparrow}^{\text{AL}}$ , say, is easily obtained by the equation of motion method

using the Hamiltonian (1) with  $t_{ij} = 0$  [6]. The result for zero field ( $h = 0$ ) is

$$G_{\uparrow}^{\text{AL}}(\epsilon) = \frac{1}{2S+1} \left[ \frac{\langle (S+S^z)n_{\downarrow} - S^{-}\sigma^{+} \rangle}{\epsilon + J(S+1)/2} + \frac{\langle (S-S^z)(1-n_{\downarrow}) - S^{-}\sigma^{+} \rangle}{\epsilon - J(S+1)/2} \right. \\ \left. + \frac{\langle (S+1+S^z)(1-n_{\downarrow}) + S^{-}\sigma^{+} \rangle}{\epsilon + JS/2} + \frac{\langle (S+1-S^z)n_{\downarrow} + S^{-}\sigma^{+} \rangle}{\epsilon - JS/2} \right] \quad (13)$$

and for  $h \neq 0$  one merely has to replace  $\epsilon$  by  $\epsilon + h/2$ . The angle brackets  $\langle \dots \rangle$  represent thermal averages and all operators within them correspond to the same site  $i$ , this suffix thus being omitted. This expression, with four poles, is considerably more complicated than the two-pole Hubbard model expression of equation (8). The poles at  $\epsilon = \pm JS/2, \pm J(S+1)/2$  correspond to energies to add or remove an electron from the atom, that is to transitions between singly-occupied states and either unoccupied or doubly-occupied states. The singly-occupied states have total spin  $S + \frac{1}{2}$  or  $S - \frac{1}{2}$  with energies  $-JS/2$  and  $J(S+1)/2$  respectively; the unoccupied and doubly-occupied states have zero energy.

In the zero-field paramagnetic case it turns out that the CPA equation for  $G(\epsilon)$  with the redundant suffix  $\sigma$  omitted, is given by equation (9) as in the Hubbard model. Thus, taking the band to have the elliptic form (10), the CPA equation for  $G$  is

$$G(\epsilon) = G^{\text{AL}}(\epsilon - W^2G/4) \quad (14)$$

with  $G^{\text{AL}}$  given by

$$G_{\uparrow}^{\text{AL}}(\epsilon) = \frac{1}{2S+1} \left[ \frac{nS/2 - \langle \mathbf{S} \cdot \boldsymbol{\sigma} \rangle}{\epsilon + J(S+1)/2} + \frac{S(1-n/2) - \langle \mathbf{S} \cdot \boldsymbol{\sigma} \rangle}{\epsilon - J(S+1)/2} \right. \\ \left. + \frac{(S+1)(1-n/2) + \langle \mathbf{S} \cdot \boldsymbol{\sigma} \rangle}{\epsilon + JS/2} + \frac{n(S+1)/2 + \langle \mathbf{S} \cdot \boldsymbol{\sigma} \rangle}{\epsilon - JS/2} \right]. \quad (15)$$

The spin symmetry of the paramagnetic state has been used to simplify the expectations in the previous form of  $G^{\text{AL}}$ , equation (13). It is easy to show that  $\langle \mathbf{S} \cdot \boldsymbol{\sigma} \rangle \rightarrow nS/2$  as  $J \rightarrow \infty$  and  $\langle \mathbf{S} \cdot \boldsymbol{\sigma} \rangle$  will be very near this limit as long as  $JS \gtrsim 2W$ . We make this approximation in calculating  $G(\epsilon)$ , and hence the density of states,  $N(\epsilon) = -\pi^{-1}\text{Im}G(\epsilon)$  from equations (14) and (15). The results are shown in figure 1 for  $S = 3/2$  and  $J = 4W$  for various  $n$ . Clearly, from equation (15), the approximation to  $\langle \mathbf{S} \cdot \boldsymbol{\sigma} \rangle$  has the effect of removing the weak band centred on  $\epsilon = -J(S+1)/2$  but it does not affect the total weight or the distribution of weight between the two lower and two upper bands. It may be seen that as  $n$  increases from 0 the band near  $\epsilon = J(S+1)/2$  is reduced in weight and a new band appears near  $JS/2$ , until at  $n = 1$  no weight remains in the band near  $J(S+1)/2$ . The weight in the band near  $-JS/2$  is  $(S+1-n/2)/(2S+1)$  per spin so if  $JS$  is sufficiently large to separate the bands ( $JS \gtrsim 2W$ ) this band will just be filled at  $n = 1$  producing a Mott insulator as expected. This redistribution of weight between bands as they fill with electrons is characteristic of the many-body CPA [24] and was missing from Kubo's one-electron CPA which was restricted to  $n = 0$ .

In the strong-coupling limit  $J \rightarrow \infty$ , which is taken with a shift of energy origin  $\epsilon \rightarrow \epsilon - JS/2$ , equation (15) simplifies to

$$G^{\text{AL}}(\epsilon) = \epsilon^{-1}(S+1-n/2)/(2S+1). \quad (16)$$

Equation (14) then becomes a quadratic equation for  $G$  with solution

$$G(\epsilon) = \alpha^2 \frac{2}{D^2} \left[ \epsilon - \sqrt{\epsilon^2 - D^2} \right] \quad (17)$$

where  $\alpha^2 = (S+1-n/2)/(2S+1)$  and  $D = \alpha W$ . By comparing with equations (10) and (11) we see that the density of states is a single elliptical band of weight  $\alpha^2$  and bandwidth  $2\alpha W$ . As

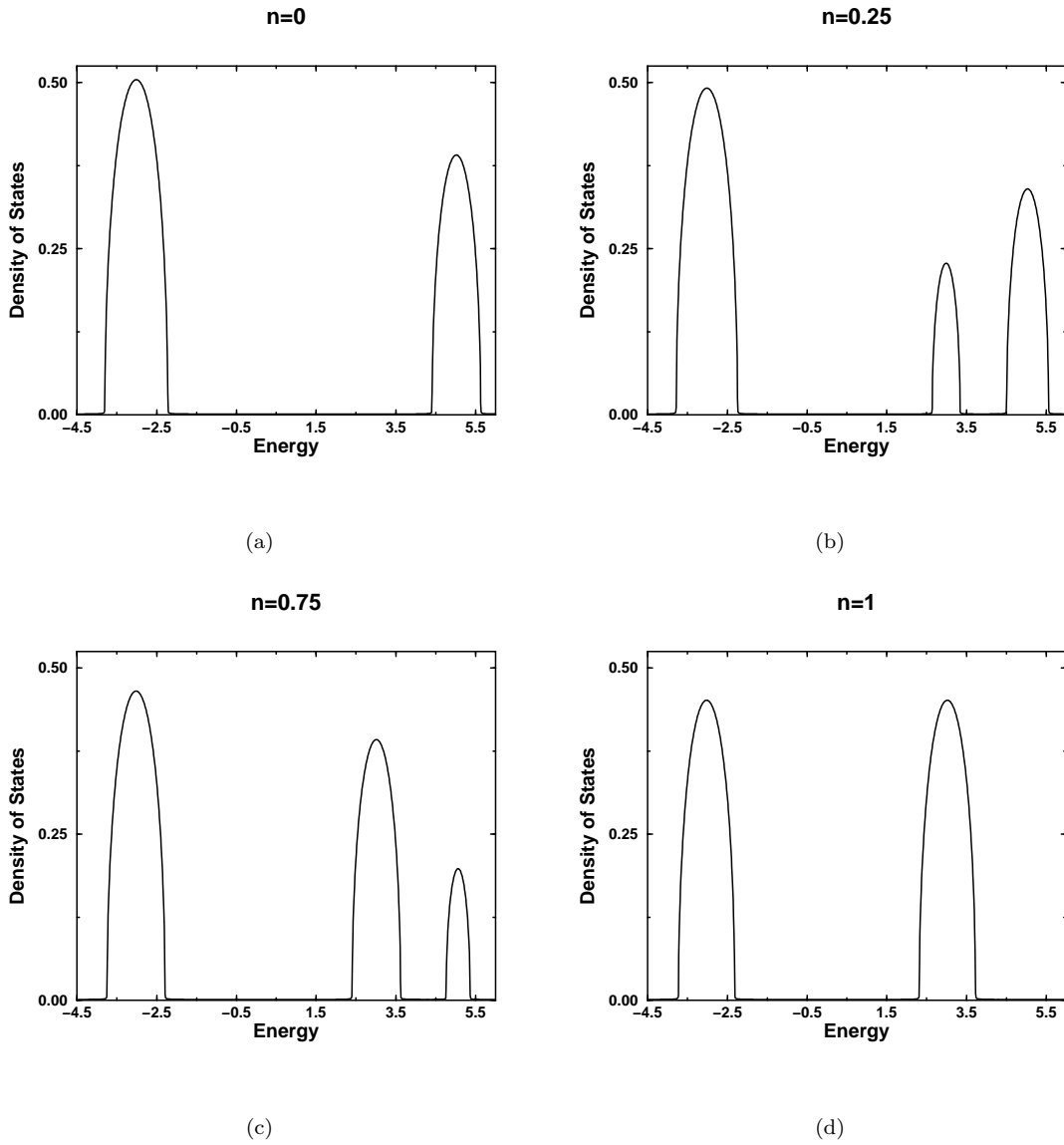


Figure 1: The density of states in the paramagnetic state of the double-exchange model for  $S = 3/2$ ,  $J = 4W$ , and  $n = 0, 0.25, 0.75$  and  $1$ . Energy units of  $W$  are used.

$S \rightarrow \infty$  the band-narrowing factor  $\alpha \rightarrow 1/\sqrt{2} = 0.707$ , which is close to the classical result of  $2/3$ , obtained by averaging  $\cos(\theta/2)$  over the solid angle.

In the classical spin limit  $S \rightarrow \infty$  we rescale  $J$ , replacing it by  $J/S$ , and the CPA equation becomes

$$G = \frac{1}{2} \left[ \frac{1}{\Sigma + G^{-1} + J/2} + \frac{1}{\Sigma + G^{-1} - J/2} \right]. \quad (18)$$

Here we have used the general equation (9), valid for arbitrary band-shape, rather than equation (14). Equation (18) is precisely the equation obtained by Furukawa [25] within DMFT.

## 4 Resistivity in the paramagnetic state of the DE model

The Kubo formula for the conductivity  $\sigma$  involves the two-particle current-current response function. However in the local approximation of CPA or DMFT there is no vertex connection and  $\sigma$  may be expressed in terms of the one-particle spectral function

$$A_{\mathbf{k}}(\epsilon) = -\pi^{-1} \text{Im} G_{\mathbf{k}}(\epsilon) = -\pi^{-1} \text{Im} [\epsilon - \epsilon_{\mathbf{k}} - \Sigma(\epsilon)]^{-1}. \quad (19)$$

In the paramagnetic state  $G$  is  $T$ -independent if we assume  $\langle \mathbf{S} \cdot \boldsymbol{\sigma} \rangle = nS/2$ , and  $\sigma$  depends on temperature only weakly through the Fermi function. If we neglect this thermal smearing around the Fermi energy  $\mu$  we may calculate at  $T = 0$  but consider the results to apply to the actual paramagnetic state at  $T > T_C$ . We find [6]

$$\sigma = \frac{2\pi e^2}{3Na^3\hbar} \sum_{\mathbf{k}} v_{\mathbf{k}}^2 [A_{\mathbf{k}}(\mu)]^2 \quad (20)$$

where  $\mathbf{v}_{\mathbf{k}} = \nabla \epsilon_{\mathbf{k}}$  is the electron velocity and  $a^3$  is the volume of the unit cell. Since  $A_{\mathbf{k}}$  depends on  $\mathbf{k}$  only through  $\epsilon_{\mathbf{k}}$  we may define a function  $\phi(\epsilon)$  such that  $\phi'(\epsilon_{\mathbf{k}}) = [A_{\mathbf{k}}(\mu)]^2$ . Hence the sum in equation (20) may be written as

$$\sum_{\mathbf{k}} \nabla \epsilon_{\mathbf{k}} \cdot \nabla \phi(\epsilon_{\mathbf{k}}) = - \sum_{\mathbf{k}} \phi(\epsilon_{\mathbf{k}}) \nabla^2 \epsilon_{\mathbf{k}}, \quad (21)$$

the last step following by means of Gauss's theorem. For a simple cubic tight-binding band  $\epsilon_{\mathbf{k}} = -2t \sum_{\beta} \cos k_{\beta} a$ , with  $\beta$  summed over  $x, y, z$ ,  $\nabla^2 \epsilon_{\mathbf{k}} = -a^2 \epsilon_{\mathbf{k}}$ . Then the summand in equation (21) is a function of  $\epsilon_{\mathbf{k}}$  only and equation (20) becomes

$$\sigma = \frac{2\pi e^2}{3a\hbar} \int dE E N_c(E) \phi(E) \quad (22)$$

where  $N_c(E)$  is the density of states for the simple cubic band. If  $N_c(E)$  is replaced by a suitably-scaled Gaussian  $N_g(E) = (3/\pi)^{1/2} W^{-1} \exp[-3(E/W)^2]$ , corresponding to an infinite dimensional approximation, equation (22) may be simplified by integrating by parts:

$$\sigma = \frac{\pi e^2 W^2}{9a\hbar} \int dE N_g(E) [A_E(\mu)]^2. \quad (23)$$

Here  $A_E(\mu)$  is defined by the right-hand expression in equation (19) with  $\epsilon = \mu$ ,  $\epsilon_{\mathbf{k}} = E$ .

Since it is convenient to use the elliptic density of states  $N_0(\epsilon)$  to calculate the Green function and self-energy, as in the previous section, it is reasonable to evaluate  $\sigma$  using equation (22) with  $N_c$  replaced by  $N_0$ . We take the strong-coupling limit  $J \rightarrow \infty$  for simplicity and the results for the resistivity  $\rho = \sigma^{-1}$  are plotted against band-filling  $n$  for various  $S$  in figure 2. We have taken  $a = 5\text{\AA}$  which is comparable with the Mn – Mn spacing in manganites. For  $J = \infty$  the band-width  $W$  is the only energy-scale and, since the integral in equation (22) is dimensionless,  $\rho$  does not depend on  $W$ . In fact in the DE regime  $JS \gtrsim 2W$  the resistivity is almost independent

of both  $J$  and  $W$ . Use of the alternative formula (23), with  $N_g$  replaced by  $N_0$ , gives very similar results. It is seen in figure 2 that  $\rho$  diverges correctly at  $n = 0$ , owing to the absence of carriers, and at  $n = 1$  where the system becomes a Mott insulator. Well away from these insulating limits  $\rho$  does not depend strongly on  $S$ , so that quantum spin effects are not very important. Furthermore  $\rho \approx 1\text{m}\Omega\text{cm}$  over a wide range of band-filling, which is much smaller than observed in some manganites above  $T_C$ , as discussed in section 7. This agrees with the conclusion of Millis et al. [14] that the DE model, with electrons scattered purely by disordered local spins, cannot describe the physics of the manganites completely. Early work by Furukawa [10] seemed to point to another conclusion, although the DMFT is equivalent to our CPA approach. We showed [6] that the confusion arose from Furukawa's use of a convenient, but rather unreasonable, Lorentzian density of states. Using a Lorentzian to replace  $N_g(E)$  and to calculate  $\phi(E)$  in equation (22) leads to a divergent integral. However equation (23) is similar to the form of  $\sigma$  used by Furukawa and use of a Lorentzian to replace  $N_c(E)$  and calculate  $A_E(\mu)$  gives a convergent result. Results of such calculations for the limit  $J \rightarrow \infty$  are shown in figure 3 and it is remarkable that  $\rho$  is at least an order of magnitude larger than one finds in figure 2 for the more reasonable elliptic band.

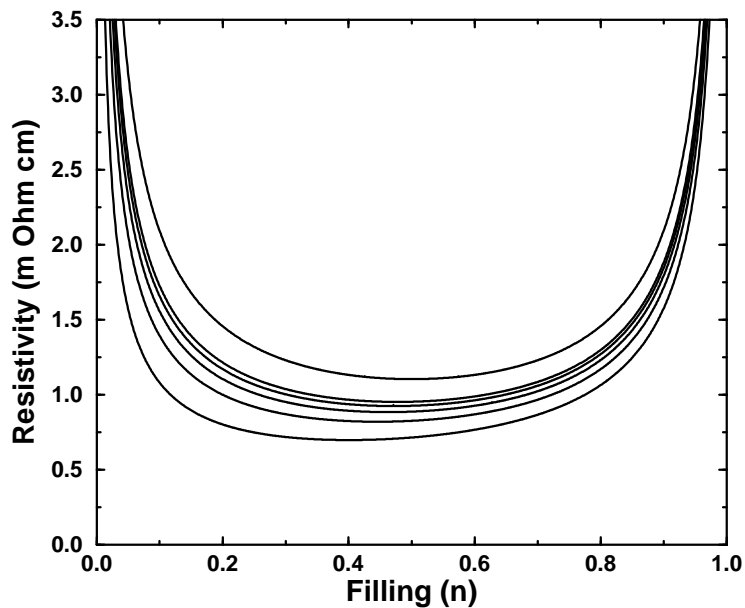


Figure 2: The zero field paramagnetic state resistivity  $\rho = \sigma^{-1}$  versus band-filling  $n$  for the double-exchange model. Here  $J = \infty$ ,  $a = 5\text{\AA}$ , and  $S = 1/2, 1, 3/2, 2, 5/2$  and  $\infty$ ,  $\rho$  increasing with  $S$ . The elliptical density of states and formula (22) are used.

## 5 Magnetism in the DE model

As discussed at the beginning of section 3, the full equation of motion approach to many-body CPA is required to determine magnetic properties such as spin susceptibility  $\chi$  and Curie temperature  $T_C$ . In our first paper [6] this involved a hierarchy of Green functions satisfying  $4S + 1$  coupled algebraic equations for local spin  $S$ ; only the  $S = 1/2$  case was briefly discussed. In a second paper [7] a major simplification was achieved by introducing generating Green functions which generate all the required Green functions by differentiation with respect to a parameter. The coupled

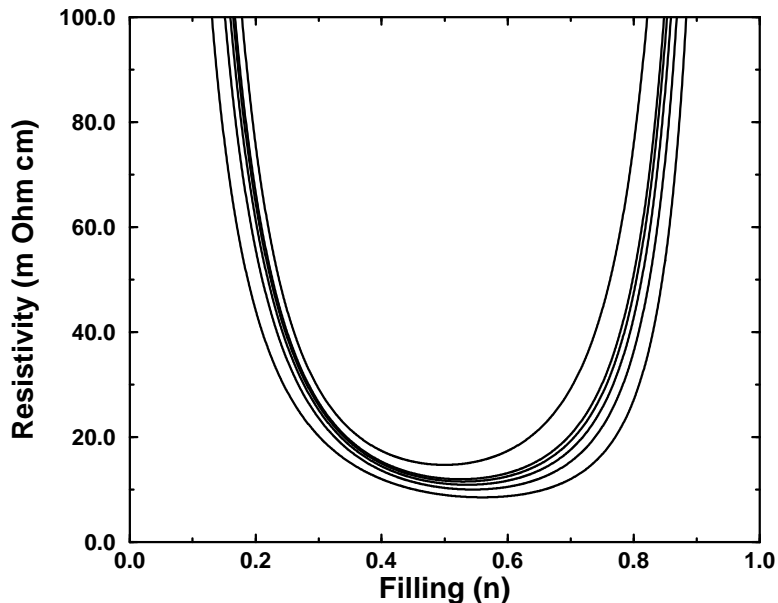


Figure 3: As in figure 2 but using a Lorentzian density of states and formula (23).

equations are then replaced by a single first-order linear differential equation, the parameter being the independent variable, whose analytic solution yields the required CPA equations for the Green functions. The classical limit  $S = \infty$  can then be taken and for  $J = \infty$  the equations coincide with those of DMFT, which are only obtainable in the classical limit. Our many-body CPA is therefore an analytic approximation to DMFT for arbitrary quantum spin  $S$  which becomes exact for  $S = \infty$ . The many-body CPA also coincides with Kubo's [24] one-electron CPA in the limit  $n \rightarrow 0$  where that is valid.

To determine the magnetic properties one problem remains; the CPA and DMFT equations contain one set of correlation functions  $\langle\langle S^z \rangle\rangle^m$  which cannot be obtained directly from the Green functions. There is an indirect procedure for determining these correlation functions within CPA but it proves to be unsatisfactory, never yielding ferromagnetic solutions. However, for  $S = \infty$ , DMFT provides a way to calculate the probability distribution function  $P(S^z)$ , and hence  $\langle\langle S^z \rangle\rangle^m$ , and we used an empirical extension of this for finite  $S$ . This extension guarantees that the spin susceptibility exhibits the correct Curie laws for band occupations  $n = 0$  and  $n = 1$ . Thus for  $n = 0$  we have a Curie law over the whole temperature range, corresponding to  $N$  independent spins  $S$ . For  $n = 1$ , with  $J = \infty$ , we have independent spins  $S + \frac{1}{2}$ . For  $0 < n < 1$  we find a finite Curie temperature  $T_C$  and some results [7] are shown in figure 4. In figure 4(a)  $T_C$  is plotted as a function of  $n$  for various  $S$  with  $J = \infty$ , using the elliptic band. Clearly for finite  $S$  ferromagnetism is more stable for  $n > 0.5$  than for  $n < 0.5$ , in agreement with the findings of Brunton and Edwards [23]. For  $S = \infty$  the result agrees closely with that of Furukawa [25]. In figure 4(b) we see the effect on  $T_C$  for  $S = 1/2$  of changing the bare band-shape from elliptic to simple cubic tight-binding. A dip in  $T_C$  occurs around  $n = 0.3$  which is the region where the ground state of the simple cubic DE model with  $S = 1/2$  is rigorously not one of complete spin alignment [23].

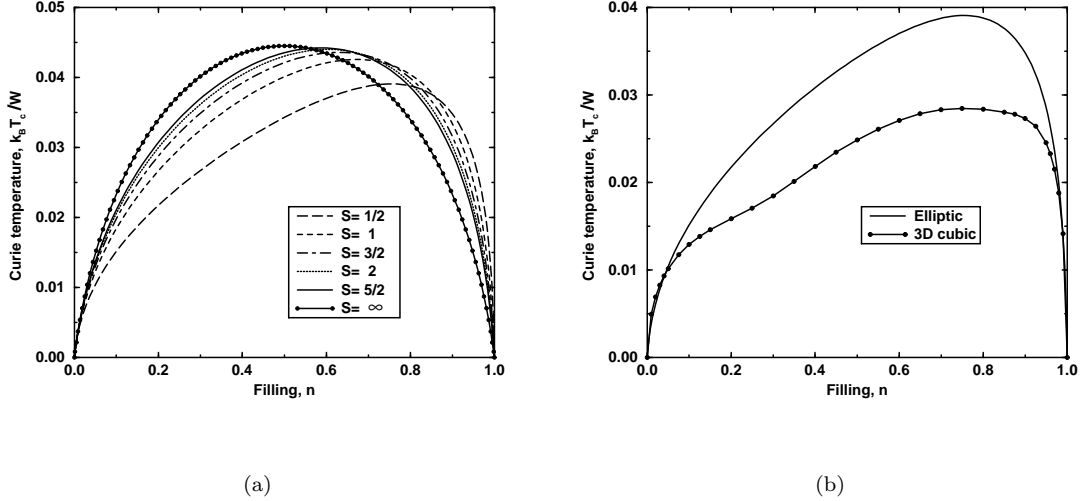


Figure 4: The Curie temperature  $k_B T_C / W$  of the double-exchange model versus band-filling  $n$  for various  $S$ , calculated with  $J = \infty$  using the elliptic band (a); the effect on  $T_C$  for  $S = 1/2$  of changing the elliptic band to the density of states for a simple cubic tight-binding band with nearest neighbour hopping (b).

## 6 Many-body CPA for the Holstein-DE model

This section is based on Green's [9] recent study of the Holstein-DE model in which the electrons of the DE model couple to local phonons as in the Holstein treatment of small polarons [26, 27]. The Hamiltonian is

$$\begin{aligned}
 H = & \sum_{ij\sigma} t_{ij} c_{i\sigma}^\dagger c_{j\sigma} - J \sum_i \mathbf{S}_i \cdot \boldsymbol{\sigma}_i - h \sum_i (S_i^z + \sigma_i^z) \\
 & - g \sum_i n_i (b_i^\dagger + b_i) + \omega \sum_i b_i^\dagger b_i.
 \end{aligned}
 \tag{24}$$

The first three terms constitute the DE Hamiltonian of equation (1) while the first, fourth and fifth terms form the Holstein model. Einstein phonons on site  $i$ , with energy  $\omega$  and creation operator  $b_i^\dagger$ , couple to the electron occupation number  $n_i = \sum_\sigma n_{i\sigma}$  with coupling strength  $g$ . The electron-phonon coupling is of the form  $-g' \sum_i n_i x_i$ , where  $x_i$  is the displacement of a shell of atoms surrounding site  $i$ , and in application to the manganites it may be regarded as an effective Jahn-Teller coupling. Previous studies of this model have either concentrated on coherent polaron bands, like Röder et al. [28], or have treated the phonons classically [12] so that there are no polaron bands at all. The many-body CPA approach is able to encompass both aspects and to describe the crossover from quantum polarons to the classical picture as temperature and/or model parameters are varied. The relationship to previous theoretical work and to experimental studies of the manganites is discussed fully in section 7. However we mention briefly below some related work on the pure Holstein model, without coupling to local spins.

Sumi considered the Holstein model with one electron in the band, first treating the phonons classically [29] and later quantum mechanically [30]. The classical case, with frozen displacements  $x_i$ , corresponds to a multicomponent alloy for which CPA is the best local approximation. In his dynamical CPA treatment of quantum phonons, Sumi [30] treated the one-site dynamics correctly and his work is completely equivalent to the more recent DMFT treatment of Ciuchi et al. [31]. As a general rule dynamical CPA and DMFT are the same for one-electron problems. DMFT is the correct extension of CPA to the many-body problem of finite electron density but for the

Holstein model, as for the DE model, it cannot be carried through analytically in the quantum case. Numerical work [32, 33] applying DMFT to the Holstein model has been aimed mostly at understanding superconducting transition temperatures and charge-density-wave instabilities rather than the polaron physics we are mainly concerned with. An unfortunate feature of the Holstein model for spin 1/2 electrons is that in a quantum treatment the true ground state for strong electron-phonon coupling consists of unphysical singlet bipolarons with two electrons bound on the same site. This problem does not occur in the one-band Holstein-DE model since strong coupling  $J$  to local spins prevents double occupation of sites, as pointed out earlier. It is also bypassed if the phonons are treated classically, as in the work of Millis et al. [33] on the Holstein model. The Holstein model is more complicated than the DE model and it turns out that our many-body CPA no longer reduces to the correct one-electron dynamical CPA/DMFT [30, 31] as band-filling  $n \rightarrow 0$ . Although correct in the atomic limit  $t_{ij} = 0$ , our theory is clearly cruder for the Holstein and Holstein-DE model than for the pure DE model.

We start by deriving the Green function for the Holstein-DE model in the atomic limit. The Hamiltonian  $H_{\text{AL}}$  in this limit is given by equation (24) with the first term omitted and with site indices and summation suppressed. We remove the electron-phonon coupling by the standard canonical transformation [34]  $\tilde{H} = e^s H_{\text{AL}} e^{-s}$  where  $s = -(g/\omega)n(b^\dagger - b)$ . Under this transformation  $b \rightarrow b + (g/\omega)n$  and the Hamiltonian separates into a fermionic and bosonic component:

$$\tilde{H} = H_{\text{f}} + H_{\text{b}} \quad (25)$$

$$H_{\text{f}} = -J\mathbf{S} \cdot \boldsymbol{\sigma} - h(S^z + \sigma^z) - (g^2/\omega)n^2, \quad H_{\text{b}} = \omega b^\dagger b. \quad (26)$$

The transformation corresponds to a displacement of the equilibrium position of the phonon harmonic oscillator in the presence of an electron and the downward energy shift  $g^2/\omega$  is a polaron binding energy which we write as  $\lambda\omega$ , where  $\lambda = g^2/\omega^2$ . If two electrons occupy the site ( $n = 2$ ), which will not occur for large  $J$ , the energy shift becomes  $4g^2/\omega^2$  corresponding to an on-site bipolaron. Writing out explicitly the thermal average in the definition of the one-particle retarded Green function we have

$$\begin{aligned} G_{\sigma}^{\text{AL}}(t) &= -i\theta(t) \left\langle [c_{\sigma}(t), c_{\sigma}^{\dagger}]_{+} \right\rangle \\ &= -i\theta(t) \frac{\text{Tr} \left\{ e^{-\beta H_{\text{AL}}} [c_{\sigma}(t), c_{\sigma}^{\dagger}]_{+} \right\}}{\text{Tr} \left\{ e^{-\beta H_{\text{AL}}} \right\}} \end{aligned} \quad (27)$$

and the canonical transformation introduced above can be carried out within the traces, using the property of cyclic invariance. Thus  $H_{\text{AL}} \rightarrow \tilde{H}$ ,  $c_{\sigma}^{\dagger} \rightarrow X^{\dagger} c_{\sigma}^{\dagger}$  and  $c_{\sigma}(t)$  becomes

$$e^{i\tilde{H}t} X c_{\sigma} e^{-i\tilde{H}t} \quad (28)$$

where  $X = \exp [g(b^\dagger - b)/\omega]$ . Using equation (25), we can write the traces in equation (27) as products of fermionic and bosonic traces. Hence we find

$$G_{\sigma}^{\text{AL}}(t) = -i\theta(t) \left\{ \langle c_{\sigma}(t) c_{\sigma}^{\dagger} \rangle_{\text{f}} F(t) + \langle c_{\sigma}^{\dagger} c_{\sigma}(t) \rangle_{\text{f}} F^{*}(t) \right\} \quad (29)$$

where  $F(t) = \langle X(t) X^{\dagger} \rangle_{\text{b}}$  and the thermal averages  $\langle \rangle_{\text{f}}$ ,  $\langle \rangle_{\text{b}}$  correspond to the systems with Hamiltonians  $H_{\text{f}}$  and  $H_{\text{b}}$  respectively. It may be shown [34] that

$$F(t) = e^{-\lambda(2b+1)} \exp \left\{ 2\lambda [b(b+1)]^{1/2} \cos [\omega(t + i\beta/2)] \right\} \quad (30)$$

where  $b = b(\omega) = (e^{\beta\omega} - 1)^{-1}$  is the Bose function with  $\beta = (k_{\text{B}}T)^{-1}$ . The last factor is of the form  $\exp(z \cos \phi)$  which generates the modified Bessel functions  $I_r(z)$ :

$$\exp(z \cos \phi) = \sum_{r=-\infty}^{\infty} I_r(z) e^{ir\phi}. \quad (31)$$

To evaluate the fermionic averages we consider for simplicity the limit  $J \rightarrow \infty$  in zero field ( $h = 0$ ). Then the last term in  $H_f$  may be written  $-(g^2/\omega)n$ , since  $n = 0$  or  $1$  only, and this may be absorbed into the chemical potential which is finally determined to give the correct number of electrons  $n$  per atom. Thus  $H_f$  is just the DE Hamiltonian in the atomic limit and the sum of the two fermionic averages corresponds to the function  $G^{\text{AL}}(t)$  whose Fourier transform is given by equation (16). It is easy to see that the first and second thermal averages in equation (29) take constant values  $(1-n)(S+1)/(2S+1)$  and  $n(S+1/2)(2S+1)$  respectively. Hence, from equations (29)-(31), we obtain the Fourier transform of  $G^{\text{AL}}$ , with  $J \rightarrow \infty$  and  $h = 0$ , in the form

$$G^{\text{AL}}(\epsilon) = \sum_{r=-\infty}^{\infty} \frac{\text{I}_r\{2\lambda[b(\omega)(b(\omega)+1)]^{1/2}\}}{(2S+1)\exp\{\lambda[2b(\omega)+1]\}} \frac{(2S+1)\frac{n}{2}e^{r\beta\omega/2} + (S+1)(1-n)e^{-r\beta\omega/2}}{\epsilon + r\omega}. \quad (32)$$

The density of states  $-\pi^{-1}\text{Im} G^{\text{AL}}(\epsilon)$  is shown in figure 5 for the classical spin limit  $S \rightarrow \infty$

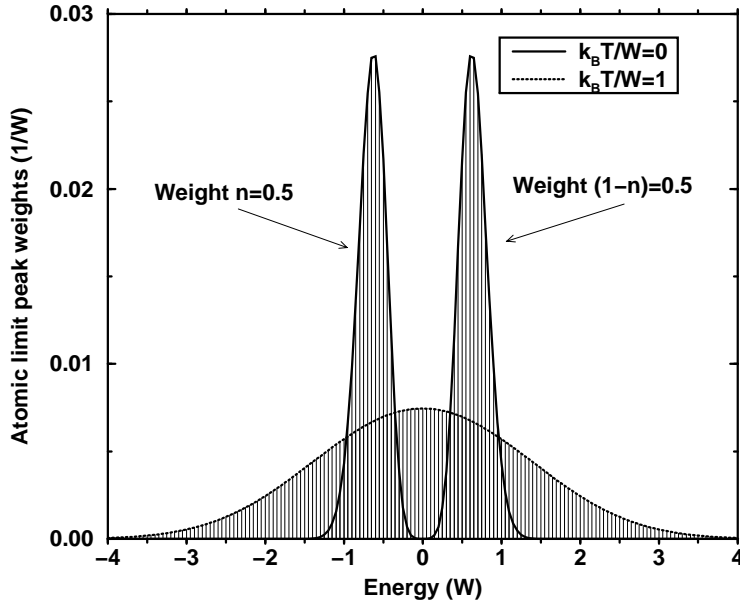


Figure 5: One-electron spectra of the Holstein-DE model in the atomic limit at zero and very high temperature. They consist of delta-functions, with energy spacing  $\omega$ , whose strength is indicated by the envelope curves. The plots are for the paramagnetic state with  $S = J = \infty$ ,  $h = 0$ ,  $n = 0.5$ ,  $\omega/W = 0.05$  and  $g/W = 0.18$ , where  $W$  is a unit of energy later to be identified with the half-width of the electron band in the full Hamiltonian.

at quarter-filling  $n = 0.5$ . It consists of delta-function peaks separated in energy by  $\omega$  and the envelope curves show the weight distribution at low and high temperature.  $W$  is an energy unit which, when we go beyond the atomic limit, will be the half-width of the itinerant electron band, as usual. The values adopted for the parameters  $\omega/W$  and  $g/W$  relate to the manganites, as discussed in section 7. The symmetry of the spectrum about zero energy is due to the choice of filling  $n = 0.5$ ; in general at  $T = 0$  the lower and upper “bands” have weights  $n$  and  $1 - n$  respectively. By counting weights it may be seen that for any  $n$  the chemical potential lies in the peak at  $\epsilon = 0$ , which has very small weight  $e^{-\lambda}/2$  per spin. The shape of the envelope function at  $T = 0$ , with two maxima and very small values at the centre of the pseudogap between them, may be understood physically as follows. The delta-function at  $\epsilon = r\omega$  ( $r \geq 0$ ) corresponds to an excitation from the ground state, with no electron and the undisplaced oscillator in its

ground state, to a state with one electron and the displaced oscillator in its  $r^{\text{th}}$  excited state. The strength of the delta-function depends on the square of the overlap integral between the displaced and undisplaced oscillator wave functions. Clearly this is very small for  $r = 0$  and goes through a maximum with increasing  $r$  as the normalized displaced wave function spreads out. At  $T = 0$  it is easily seen from equation (32), using  $I_r(z) \sim (z/2)^{|r|}/|r|!$  for small  $z$ , that the weight of the delta-functions at  $\epsilon = \pm r\omega$  is proportional to  $\lambda^r/r!$ . Hence the maxima in the envelope curve occur at  $\epsilon \approx \pm\lambda\omega$ , which is the polaron binding energy.

We now turn to the Holstein-DE model with finite band-width. As for the DE model it is necessary to use the full equation of motion method to derive the many-body CPA in the presence of a magnetic field and/or magnetic order [9]. In the present case it is very difficult to determine self-consistently all the expectation values which appear. We therefore approximate them by their values in the atomic limit. It then turns out that in the zero field paramagnetic state, for  $J = \infty$  and with the elliptic band, the CPA Green function  $G$  again satisfies equation (14), with  $G^{\text{AL}}$  now given by equation (32).

The densities of states calculated for  $T = 0$  using equations (32) and (14) with  $S = \infty$ ,  $n = 0.5$ ,  $\omega/W = 0.05$  and various values of  $g/W$  are shown in figure 6. Apart from lacking the perfect symmetry about the chemical potential  $\mu = 0$  the results are qualitatively similar for other values of  $n$  not too close to 0 or 1. For  $g = 0$  we recover the elliptic band with half-width  $W/\sqrt{2}$  as for the DE model with  $J = \infty$ ,  $S = \infty$ . As  $g$  increases the density of states broadens and small subbands are split off from the band edges. As  $g$  increases further a pseudogap develops near the chemical potential. At a critical value  $g = g_c$  a gap appears which contains a small polaron band around the chemical potential. Increasing  $g$  further causes more bands to be formed in the gap, with weights similar to those of the relevant atomic limit. It should be pointed out that the paramagnetic state considered here at  $T = 0$  is not the actual ground state, which is ferromagnetic. We discuss the magnetic state later. The effect of increasing temperature on the density of states in the gap region is shown in figure 7 for  $g = 0.18W > g_c$ . With increasing  $T$  the polaron bands grow rapidly and eventually merge to fill the gap.

It is important to compare these results with the standard small polaron theory developed by Holstein [25, 33]. Holstein distinguished between “diagonal transitions”, in which the number of phonons is unchanged as the electron moves from site to site, and “nondiagonal transitions” in which phonon occupation numbers change. The former give rise to a coherent Bloch-like polaron band of half-width  $We^{-\lambda(2b+1)}$  which decreases with increasing temperature. The nondiagonal transitions are inelastic processes which destroy phase coherence and the polaron moves by diffusive hopping. The hopping probability increases with temperature so that polaron motion crosses over from coherent Bloch-like at  $T = 0$  to diffusive hopping as  $k_{\text{B}}T$  approaches the phonon energy  $\omega$ . The paramagnetic state of the Holstein-DE model differs from this standard picture in one important respect. There are no well-defined Bloch states, owing to strong scattering by the disordered local spins, so no coherent polaron band will form. This is fortunate because the CPA treatment of electron-phonon scattering will never lead to coherent states of infinite lifetime at the Fermi surface at  $T = 0$ . However in the presence of strong spin disorder it should be satisfactory. We interpret the central band around the chemical potential in figure 7 as an incoherent polaron band whose increasing width as the temperature rises is due to life-time broadening of the atomic level. The life-time decreases as the hopping probability increases with rising temperature.

To substantiate this picture we study the central polaron band in the limit of very strong electron-phonon coupling. In this limit it can be shown that we need retain only the  $r = 0$  term in equation (32) and it is then easy to solve equation (14) for  $G$ . The result is of the same form as equation (17) but with

$$D^2 = \frac{1}{2}W^2e^{-\lambda(2b+1)}I_0\left(2\lambda[b(b+1)]^{1/2}\right). \quad (33)$$

The central band is thus elliptical with half-width  $D$  and weight  $D^2/W^2$ . It is now easy to calculate

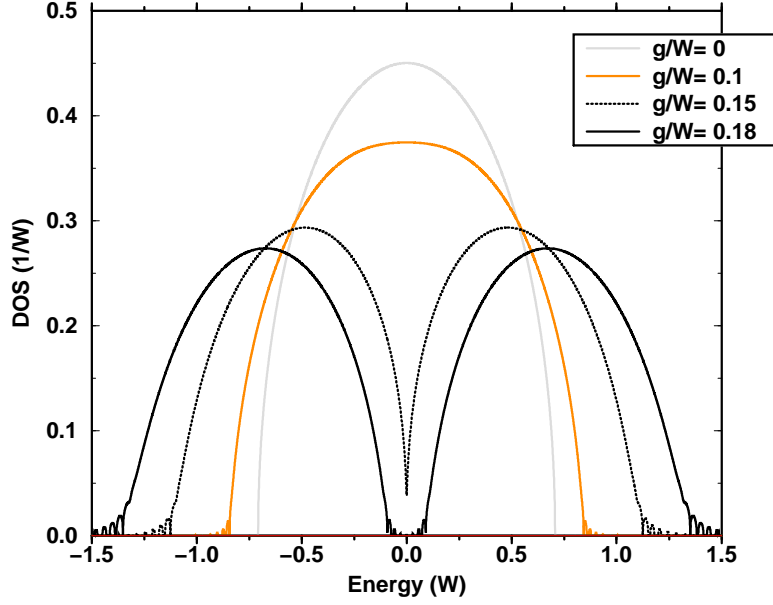


Figure 6: The one-electron density of states (DOS) for the Holstein-DE model with half-bandwidth  $W$ , for the hypothetical paramagnetic state at  $T = 0$ , with various strengths of electron-phonon coupling  $g/W$ . Other parameters as in figure 5.

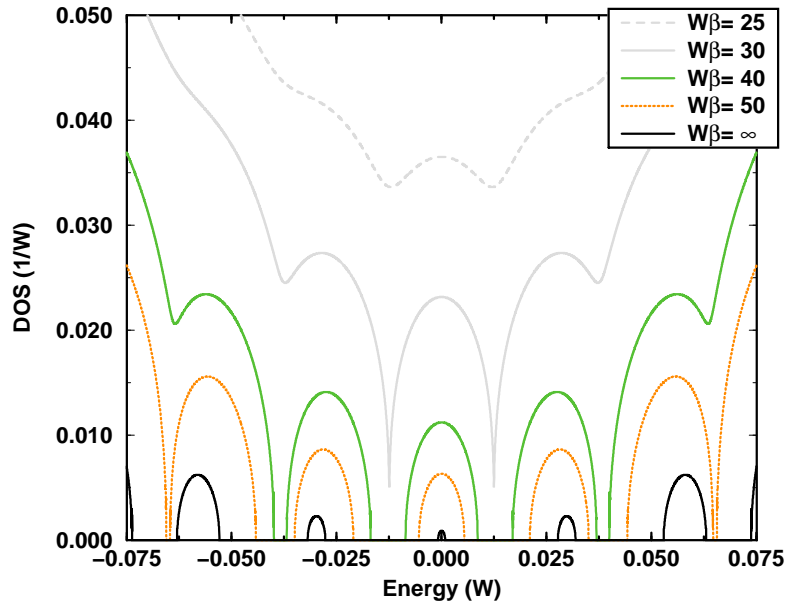


Figure 7: Evolution with temperature  $\beta = (k_B T)^{-1}$  of the polaron subbands in the pseudogap around the chemical potential  $\mu = 0$  for  $g/W = 0.18$ . These subbands at  $T = 0$  can just be seen in figure 6. All parameters as in figure 5.

the conductivity  $\sigma$  from equation (20) and, using  $D^2 \ll W^2$ , we find

$$\sigma = \frac{\pi e^2}{6\hbar a} \frac{D^2}{W^2} \approx \frac{\pi e^2}{12\hbar a} \left( \frac{\beta\omega}{4\pi\lambda} \right)^{1/2} e^{-\beta\lambda\omega/4}. \quad (34)$$

The last step follows by using the asymptotic forms for strong coupling and high temperature  $I_0(z) \sim (2\pi z)^{-1/2} \exp z$  and  $b \sim (\beta\omega)^{-1}$ . The temperature dependence of  $\sigma$  is the same as in the standard theory of small polaron hopping conduction [34] but with activation energy  $\lambda\omega/4$  equal to one quarter, instead of one half, of the polaron binding energy. The standard result is for one electron coupled to the lattice without spin disorder. Nevertheless this establishes the link between our work and standard small polaron theory in the strong coupling limit. However the results shown in figure 7, with parameters relevant to typical manganites, are far from this limit. They correspond to intermediate coupling and in the actual paramagnetic state above the Curie temperature the polaron bands are largely washed out. In this regime, with increasing temperature, there is a crossover from polaronic behaviour to a situation where the phonons behave classically, the case considered by Millis et al. [12]. For electron-phonon coupling greater than a critical value these authors find a gap in the density of states which gradually fills with increasing temperature. However in their classical treatment there are no polaron bands in the gap so that the link with standard polaron physics is not established.

Apart from the symmetry about  $\epsilon = 0$  the above results for  $n = 0.5$  are not untypical of the general case. For general  $n$  the main lower and upper bands, separated by a gap for  $g > g_c$ , have approximate weights  $n$  and  $1 - n$  respectively. The chemical potential at  $T = 0$  is always confined to the polaron band arising from the  $r = 0$  term of equation (32), and moves from the bottom at  $n = 0$  to the top at  $n = 1$ , so that we correctly have an insulator in these limits.

To calculate the Curie temperature  $T_C$  we need the full CPA theory combined with an exact result of DMFT for  $S = \infty$  [9]. Results on  $T_C$  for the same parameters as before are plotted as functions of electron-phonon coupling  $g$  in figure 8. The suppression of  $T_C$  with increasing  $g$  was first noted by Röder et al. [28] and our own results are quite similar to those of Millis et al. [12]. In our CPA we have no reliable means of calculating the probability distribution function  $P(S^z)$ , so to go below  $T_C$  we use the mean-field approximation for the ferromagnetic Heisenberg model with classical spins and nearest neighbour exchange. The exchange constant is determined by  $T_C$ . We plot the up- and down-spin density of states for  $T = 0.005W/k_B \ll T_C$  and  $g = 0.16W > g_c$  in figure 9, also showing curves for the saturated ferromagnetic state and paramagnetic state at  $T = 0$  for comparison. The value  $g = 0.16W$  is closer to  $g_c$  than the value of  $0.18W$  used in figures 6 and 7 and we discuss these results in relation to the manganites in the next section. In figure 9 we plot the resistivity  $\rho$  as a function of temperature, for the same parameter set, with different applied fields  $h$ . The resistivity peaks sharply at  $T_C$ , and for comparison we show results for weaker electron-phonon coupling  $g/W = 0.10$  in figure 11. The curve in figure 11 is almost indistinguishable from that of figure 7 in reference [9] for  $g/W = 0.01$ . This is not surprising since we see from figures 6 and 8 of this paper that the density of states and  $T_C$  change very little between  $g/W = 0$  and  $g/W = 0.1$ . These results are all discussed further in the next section.

## 7 Application to manganites

Much experimental work has concentrated on the systems  $\text{La}_{1-x}\text{Ca}_x\text{MnO}_3$  and  $\text{La}_{1-x}\text{Sr}_x\text{MnO}_3$  with  $x \approx 0.33$ , in the middle of the ferromagnetic regime where CMR is observed. For brevity we denote these systems by LCMO and LSMO respectively. In comparing experiments with the detailed results of section 6 it should be borne in mind that the deduced parameters will be influenced by our convenient choice of  $n = 1 - x = 0.5$  rather than  $n = 0.6 - 0.7$ . However the correct general picture should emerge. Since we consider a homogeneous state we are not concerned with the existence of charge ordering for  $x = 0.5$ . We should also discuss the effect of using a one-band model for the  $e_g$  band, rather than the more realistic two-band model. An important point to notice is that in the two-band model large Hund's rule coupling  $J$  to the local spins

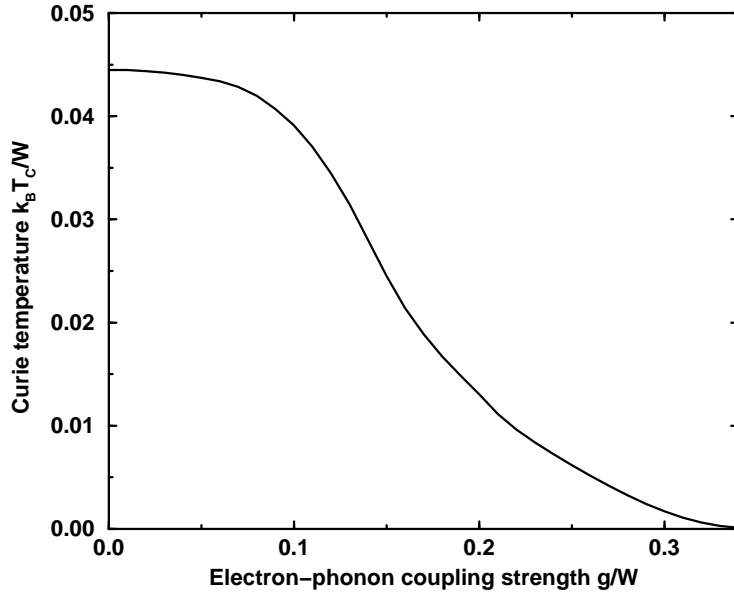


Figure 8: Suppression of the Curie temperature of the Holstein-DE model with increasing electron-phonon coupling  $g/W$ . The plot is for  $S = J = \infty$ ,  $h = 0$ ,  $n = 0.5$  and  $\omega/W = 0.05$ .

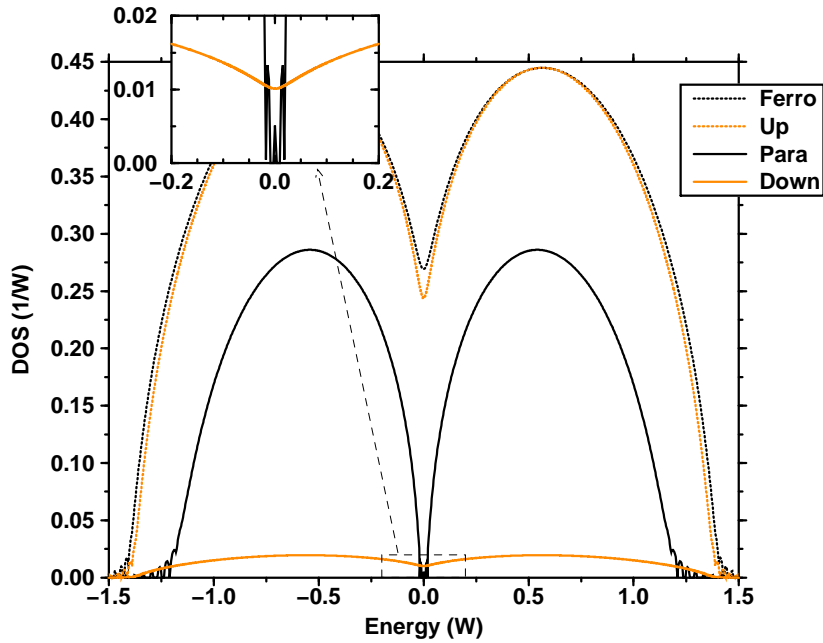


Figure 9: The up- and down-spin density of states of the Holstein-DE model with  $g/W = 0.16$  for  $k_B T = 0.005W \ll k_B T_C$  where  $\langle S^z \rangle = 0.915$ . Also shown are the DOS for the saturated ferromagnetic state at  $T = 0$  and for the hypothetical paramagnetic state at  $T = 0$ . All plots are for  $S = J = \infty$ ,  $h = 0$ ,  $n = 0.5$ ,  $\omega/W = 0.05$  and  $g/W = 0.16$ .

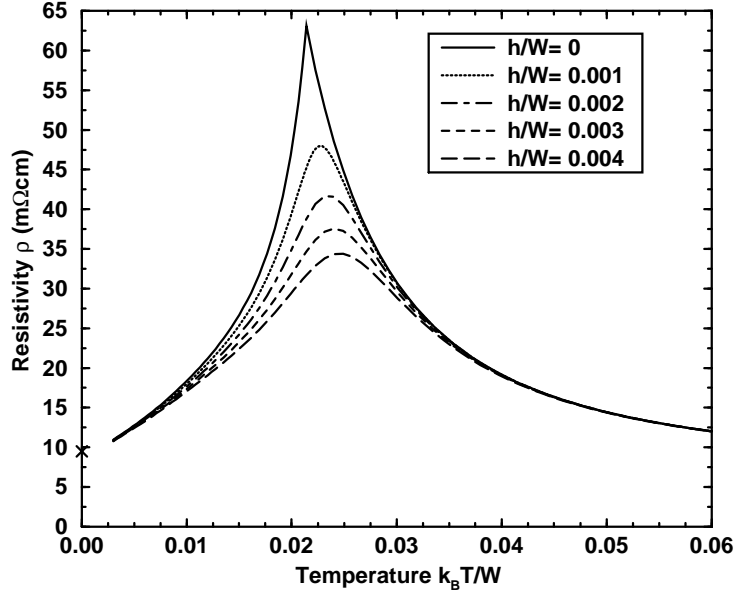


Figure 10: Resistivity  $\rho$  versus temperature for the Holstein-DE model with  $S = J = \infty$ ,  $n = 0.5$ ,  $\omega/W = 0.05$ , intermediate coupling  $g/W = 0.16$  and various applied fields  $h$ . The lattice constant is taken as  $a = 5\text{\AA}$ , slightly larger than the Mn – Mn spacing in the manganites.

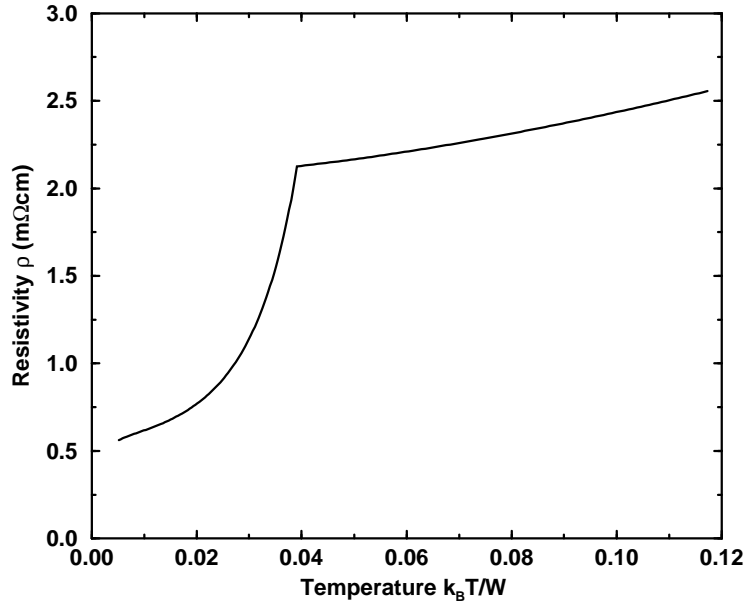


Figure 11: The same plot as figure 10 but for weak electron-phonon coupling  $g/W = 0.10$ .

no longer produces a Mott insulator for  $n = 1$  and it is necessary to introduce on-site Coulomb interaction [35, 36]. Millis et al. [12] do not do this so that for  $n = 1$ , which should correspond to the undoped insulator, they have a metal. Also, for weak electron-phonon interaction, they find  $T_C$  is largest for this value of  $n$ . This contrasts strongly with figure 4 where, in the one-band DE model,  $T_C = 0$  at  $n = 0$  and 1 and has a maximum in between. Held and Vollhardt [36], using DMFT, obtain very similar results to ours for  $S = \infty$  in the two-band model with strong on-site Coulomb interaction included. However their values of  $T_C$  are about twice ours. Nevertheless we conclude that the one-band DE and Holstein-DE models may sensibly be used to discuss the manganites. We see from figures 2 and 4 that for the DE model neither  $T_C$  nor the resistivity  $\rho$  vary enormously with  $S$  so that  $S = \infty$  is a reasonable approximation to the  $S = 3/2$  Mn spin. It is also reasonable to take the DE limit  $J \rightarrow \infty$  [37]. For comparison with experiment we take  $W = 1$  eV which band calculations [38, 37] suggest as an appropriate half-bandwidth for the  $e_g$  band. Also in figures 6-11 we have taken  $\omega/W = 0.05$  to correspond to observed transverse optic phonons with  $\omega \approx 40 - 70$  meV which couple strongly to the electrons in LCMO [39].

Perhaps the most striking feature of the manganites is the very different behaviour observed in apparently similar materials such as LSMO and LCMO. For LSMO, with  $x \approx 0.33$ ,  $T_C \approx 370$  K whereas for LCMO, with a similar  $x$ ,  $T_C \approx 240$  K. The difference in behaviour of the resistivity  $\rho$  above  $T_C$  is much more striking. For LSMO  $\rho \approx 4$  m $\Omega$  cm and increases slowly with temperature as in a poor metal [40]. The  $\rho(T)$  curve is very similar to that of figure 11 for  $g/W = 0.1$  except for a much larger resistivity at low temperature in our calculations. Since this feature persists even for  $g/W = 0.01$  (figure 7 in reference [9]) it presumably arises from overestimated spin disorder scattering at low temperatures due to our use of the classical spin Heisenberg model to determine  $P(S^z)$ . In LCMO the resistivity rises to a maximum at  $T_C$  of about 40 m $\Omega$  cm and then falls with increasing temperature above  $T_C$  [41]. In contrast to LSMO there is thus a transition from metallic to insulating behaviour. Also the resistivity peak is strongly reduced and shifted to higher temperature with increasing applied magnetic field. This is the CMR effect. This type of behaviour is seen in figure 10 for  $g/W = 0.16$ . The main differences between theory and experiment are a more rapid observed drop in  $\rho$  with decreasing temperature below  $T_C$  and a more sensitive observed CMR effect.  $h/W = 0.004$  corresponds to a field of about 20 T for  $W = 1$  eV and the corresponding reduction in  $\rho$  in figure 10 is achieved with a field of about 5 T experimentally. Millis et al. [12] noted a similar problem in their work using classical phonons. Both of the discrepancies mentioned might be remedied by introducing a dependence of  $g$  on  $\rho$ , corresponding to more efficient screening of the electron-phonon interaction with increasing metallization. The huge reduction in resistivity peak on reducing from  $g/W$  from 0.16 to 0.10 shows the extreme sensitivity of  $\rho$  to changes in  $g$ . The main point to notice is that we can understand the enormous difference between LCMO and LSMO within our theory by assuming the electron-phonon coupling changes from  $g/W = 0.16$  in LCMO to  $g/W = 0.10$ , or slightly greater, in LSMO. The observed ratio of the Curie temperatures, slightly less than 2, is then in accord with figure 8. As discussed in section 6 the critical coupling  $g_c$  for the formation of a polaron band is  $g_c/W \approx 0.15$ , with our phonon energy  $\omega/W = 0.05$ , and to obtain the right order of magnitude for  $\rho$  above  $T_C$  in LCMO,  $g$  is pinned down closely to 0.16. A larger value for  $g$  leads to too high a resistivity and too low a Curie temperature. It is interesting that neither  $\rho(T)$  nor  $T_C$  change when  $g/W$  is varied between 0.1 and 0. This means that LSMO can be described very well by the pure DE model, as stressed by Furukawa [25], but it does not follow that electron-phonon coupling is negligible. However, from the results of Millis et al. [12] for classical phonons, one can understand why a coupling small enough to give a LSMO-like  $\rho(T)$  curve does not lead to a change in slope of the rms oxygen displacements, as a function of temperature, at  $T_C$ . No such change is found in LSMO [42], in contrast to the case of LCMO [43]. It is more difficult to understand the observation [44] of static local Jahn-Teller distortions in LSMO at room temperature, apparently associated with localized carriers in the presence of metallic conduction.

From figures 6 and 9 we see that for  $g/W = 0.1$ , appropriate to LSMO, there is no sign of a pseudogap in the density of states. An actual gap in the hypothetical paramagnetic state at  $T = 0$  appears at  $g = g_c$  with  $g_c$  between 0.15 and 0.16. From figure 9 we see that for  $g/W = 0.16$ , appropriate to LCMO, a few polaron subbands have appeared in the gap. These are seen much

more clearly in figure 7 for  $g/W = 0.18$  when there is a larger gap. However the subband structure is washed out completely for  $\beta W = 25$ , corresponding to  $T = 464$  K for  $W = 1$  eV, and this effect will occur at a much lower temperature for  $g/W = 0.16$ . Thus in the actual paramagnetic state of LCMO above  $T_C$  we do not expect the quantum nature of phonons to manifest itself, so we are essentially in the classical regime of Millis et al. [12]. The same is true in the saturated ferromagnetic state at  $T = 0$  where only a pseudogap appears in figure 9. As the temperature rises towards  $T_C$  a minority spin band grows, also with a pseudogap, while the majority spin band loses weight. The width of the ferromagnetic bands decreases with increasing temperature, corresponding to the DE effect, but the narrowing in the paramagnetic state is not so marked as in the pure DE model. Thus double exchange is not so effective in the presence of strong electron-phonon coupling, which is consistent with the reduction in  $T_C$  shown in figure 8.

Clearly our picture of the manganites is close in spirit to that of Millis et al. [12], although the relationship to polaron physics is not so clear in their classical approximation. Other authors adopt completely different viewpoints. Furukawa [25] rejects the importance of electron-phonon coupling and argues in favour of phase separation models of LCMO with, for example, ferromagnetic and charge-ordered regions. Such scenarios have been extensively discussed by the Florida group [45, 46]. It is controversial whether such phase separation can occur for  $x \approx 0.33$  which is far from the antiferromagnetic insulating phase near  $x = 0$  and the region with charge and orbital ordering near  $x = 0.5$ . Nagaev [47] also argues against any polaronic effects, while Alexandrov and Bratkowsky [48, 49] assume strong electron-phonon coupling with small polarons even in the ferromagnetic state and with immobile bipolarons forming near  $T_C$ . The public correspondence [50, 49] between Nagaev and Alexandrov and Bratkowsky (AB) centres on estimating the magnitude of the polaron binding energy  $E_p$  and the criterion for small polaron formation [51]. Since our picture of LCMO lies between their extreme views it is interesting to compare our estimates with theirs. For LCMO we find  $E_p = g^2/\omega \approx 0.5$  eV for  $W = 1$  eV whereas, for manganites in general, Nagaev estimates  $E_p \approx 0.1 - 0.3$  eV and AB estimate  $E_p \approx 1$  eV. Our condition for small-polaron formation in a paramagnetic state at  $T = 0$  is  $g > g_c \approx 0.15W$  which corresponds to  $E_p > 0.45W$ . Nagaev adopts the criterion  $E_p > W$ , remembering that  $W$  is the half-bandwidth in our notation, while AB [51] propose  $E_p > 2W(8z)^{-1/2} = 0.29W$  with number of nearest neighbours  $z$  taken as 6. AB's condition is less stringent than Eagle's [52] condition for "nearly small polarons"  $E_p > Wz^{-1/2} = 0.41W$  which is close to ours. Both as regards this criterion and the value of  $E_p$  for LCMO, our results are intermediate between Nagaev's and AB's, as expected. For LSMO, on the other hand, our estimate of  $E_p$  is 0.2 eV. In this case we agree with Nagaev that electron-phonon coupling is not important. AB assume stronger electron-phonon coupling than we find in LCMO. Hence they have a coherent small-polaron band in the ferromagnetic state which apparently supplies the required metallic conductivity. The carriers are unable to bind to form singlet bipolarons.

AB [48, 49] assume that the strong Hund's rule coupling, which we and most authors assume is effectively infinite, can be treated in mean field theory. Instead of the double-exchange effect, in which the occupied polaron band merely narrows as its weight redistributes between up and down spin, the Hund's rule exchange splitting collapses above  $T_C$  and it is assumed that immobile singlet bipolarons can form. Hence near  $T_C$  there is an enormous increase in resistivity which decreases above  $T_C$  as the bipolarons dissociate. The problem with this theory as it stands, even more serious than doubts about the existence of polarons above and below  $T_C$ , is the mean field treatment of the large Hund's rule exchange.

The giant isotope effect observed in LCMO and  $\text{Nd}_{0.7}\text{Sr}_{0.3}\text{MnO}_3$  has been interpreted as evidence for immobile bipolaron formation [53]. The effect is seen as a decrease of  $T_C$  and a big increase in resistivity, particularly near  $T_C$ , when  $^{16}\text{O}$  is replaced by  $^{18}\text{O}$ . To investigate this effect in our model some care is needed. It was pointed out that in equation (24) the electron-phonon coupling term corresponds to a term  $-g' \sum_i n_i x_i$  where  $x_i$  is to be associated with oxygen displacement around a Mn atom. Here  $g'$  should be independent of the oxygen mass  $M$ . In the second-quantized form of equation (24) one finds  $g = g' (2M\omega)^{-1/2}$  so that the polaron binding energy  $g^2/\omega = g'^2 / (2M\omega^2)$ . Since for an oscillator  $\omega \propto M^{-1/2}$  the polaron binding energy  $g^2/\omega$

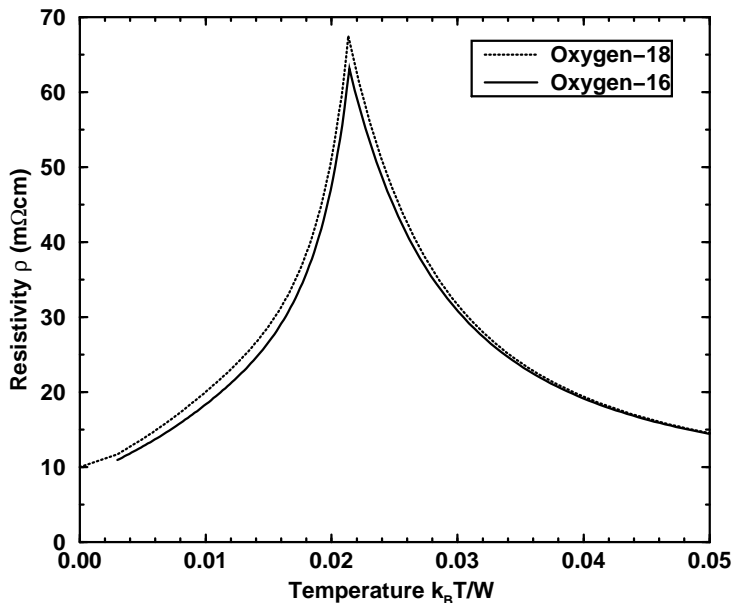


Figure 12: The absence of an isotope effect in LCMO due to a simple mass scaling ( $\propto M^{1/2}$ ) of the phonon frequency.

is expected to be independent of  $M$ . However  $g$  varies as  $M^{-1/4}$ . We have therefore recalculated the resistivity  $\rho(T)$  with the same parameters as used in figure 10 for  $^{16}\text{O}$  but with  $g$  and  $\omega$  scaled appropriately for  $^{18}\text{O}$ . The results are compared in figure 12. The almost complete absence of an isotope effect in both  $T_C$  and  $\rho$  is remarkable in view of the moderately strong electron-phonon coupling in our model of LCMO. Since we do not believe in the bipolaron theory for LCMO another explanation of the isotope effect must be sought. Nagaev has considered several possibilities, all based on the isotope dependence of the number of excess or deficient oxygen atoms in thermodynamic equilibrium [47, 54]. In LCMO with  $x = 0.2$  there is experimental evidence that at least part of the isotope effect is due to varying oxygen content [55]. A change in oxygen nonstoichiometry could lead to a change in carrier density and, perhaps due to volume change, to a change in electron-phonon coupling  $g'$ . In view of the sensitivity of  $\rho(T)$  to electron-phonon coupling we think that the isotope effect may be due more to a change in  $g'$ , or to a change in  $\omega$  beyond the simple mass scaling, than to a change in  $n$ . Since Nagaev believes electron-phonon coupling to be unimportant he did not consider this particular consequence of his nonstoichiometry proposal. The involvement of electron-phonon coupling in the isotope effect would explain why the  $T_C$  shift in LSMO is much smaller than in LCMO [56]. To illustrate such a mechanism we have recalculated  $\rho(T)$  for the  $^{18}\text{O}$  system with scaled  $\omega$  as before ( $\propto M^{-1/2}$ ) but with  $g$  unchanged from its  $^{16}\text{O}$  value. This implies a 3% increase in  $g'$ . The results are shown in figure 13. In the paramagnetic state they are quite similar to those observed in LCMO with  $x = 0.25$  and in  $\text{Nd}_{0.7}\text{Sr}_{0.3}\text{MnO}_3$ . The only conclusion we can draw from this arbitrary calculation is that it may be extremely difficult to determine the true origin of the isotope effect in such a critical system as LCMO on the verge of small-polaron formation. However it does not arise from a simple mass scaling of the phonon frequency.

Another example of the sensitivity of  $\rho$  to variation in parameters is the effect of pressure [57]. The strong suppression of the resistivity peak and the increase in Curie temperature in LCMO can be modelled within our theory by increasing the bandwidth [9], and assuming other terms in the Hamiltonian are constant. Calculated results are shown in figure 14. This pressure effect

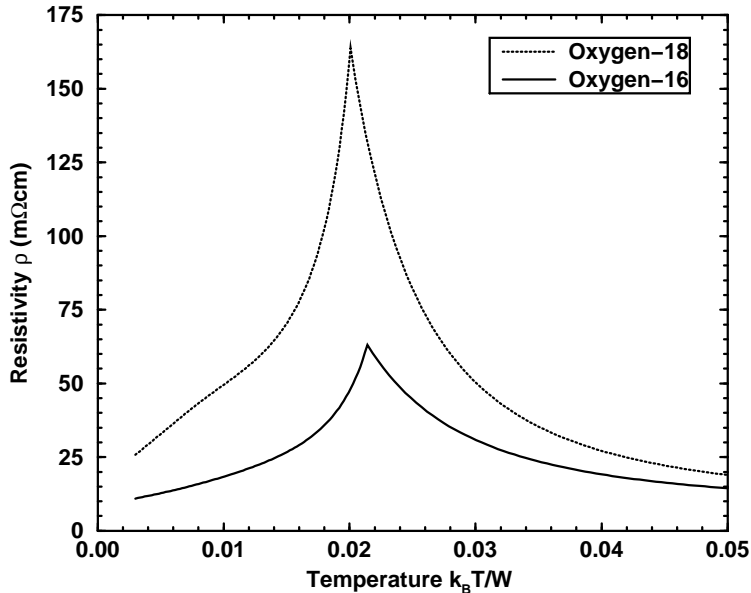


Figure 13: A giant isotope effect due to mass scaling of the phonon frequency together with a 3% increase of electron-phonon coupling strength in the  $^{18}\text{O}$  system. This arbitrary modelling shows how an effect similar to that observed [53] might arise from small parameter changes associated with changed oxygen content.

is due to a reduction in  $g^2/(\omega W)$ , the ratio of polaron binding energy to the half-bandwidth. A simple estimate, using the known compressibility and dependence of  $W$  on lattice constant, shows that the theoretical pressure for a given effect is about four times larger than that required experimentally. This is the same factor that we found in the case of the magnetic field required for a given CMR effect, so both discrepancies could possibly be removed with the same dependence of  $g$  on  $\rho$ , due to screening, postulated earlier.

According to our theory we expect pseudogaps at the Fermi level to be observable in the density of states of LCMO both below and above  $T_C$ . These should appear in experiments such as scanning tunnelling spectroscopy, photoemission and optical conductivity measurements. No pseudo gaps are expected in LSMO. The pseudogap is a feature of the atomic limit, typified by the envelope function in figure 5 for  $T = 0$  with maxima determined by the polaron binding energy  $g^2/\omega$ , and is completely washed out when  $g^2/(\omega W) < 0.2$  (see figure 6). Early results of scanning tunnelling spectroscopy on LCMO [58] with  $x = 0.3$  seem unlikely to relate to the bulk. In the ferromagnetic state at 77 K there is a huge gap of about 1 eV. It is not clear why the authors interpret this as evidence for half-metallic ferromagnetism. A gap of this size associated with small-polaron formation in the bulk would imply an unrealistically large electron-phonon coupling, certainly incompatible with metallic conduction and a Curie temperature of reasonable magnitude for LCMO. More recently Biswas et al. [59] reported a scanning tunnelling spectroscopy study of several manganites. The results are very much in accord with our theory. There is no gap in the low temperature ferromagnetic state but a small gap (pseudogap) appears for  $T \approx T_C$  in the low (high)  $T_C$  materials. As  $T$  increases above  $T_C$  the pseudogap or gap gets filled in as we would expect (see figure 7).

In an extremely interesting paper on angle-resolved photoemission spectroscopy for the bilayer manganite  $\text{La}_{1.2}\text{Sr}_{1.8}\text{Mn}_2\text{O}_7$ , nominally with  $n = 0.6$ , Dessau et al. [60] interpret their results very much in the spirit of our theory. In this layered structure we cannot estimate the strength of

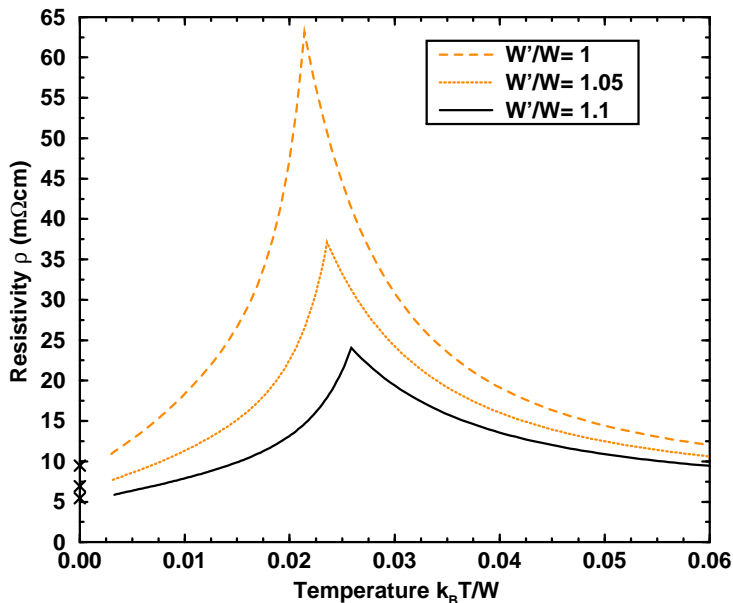


Figure 14: The effect of pressure on the resistivity and Curie temperature in LCMO by increasing the half-bandwidth  $W$  to  $W' = 1.05W$  and  $1.1W$ .

the electron-phonon coupling from  $T_C$ , whose low value of 126 K is largely a result of quasi-two dimensional fluctuations. However the large low-temperature resistivity of more than  $3 \text{ m}\Omega \text{ cm}$  suggests that small-polaron bands might exist in both the ferromagnetic and paramagnetic state. This indicates a larger value of  $g/W$  than in the cubic manganites, which might be expected from a reduced bandwidth in the layered structure. In this case the polaron bands would not be washed out above  $T_C$  and should exist within a wider gap than in the ferromagnetic state. This is compatible with the observations. Dessau et al. [60] interpret the widths of their  $\mathbf{k}$ -resolved spectral peaks in terms of multiple polaron subbands. The fact that strong peaks all occur at  $0.65 - 1.0 \text{ eV}$  below the Fermi level, independent of  $\mathbf{k}$ , suggests that the system is not so far from the atomic limit, with the spectral peaks given by the envelope function in figure 5 for  $T = 0$ . This indicates a large polaron binding energy of  $0.65 - 1.0 \text{ eV}$  and Alexandrov and Bratkovsky have applied their theory [51] to these bilayer manganites. They interpret the observed upward shift in frequency  $\nu$  of the maximum in the optical conductivity  $\sigma(\nu)$ , between 10 K and just above  $T_C$ , as due to bipolaron formation. We cannot discuss the possible binding of two polarons on nearest-neighbour sites within our local approximation. However one does not need bipolarons to understand an upward shift of the optical conductivity maximum with increasing temperature. This is clearly seen already in the calculations of Millis et al. [12] where the phonons are treated classically. In connection with the work of Dessau et al. [60], it should be mentioned that Moreo et al. [61] interpret the observed pseudogap not as an intrinsic property but in terms of phase separation.

Kim et al. [62] have reported very interesting measurements of optical conductivity  $\sigma(\nu)$  in  $\text{La}_{0.7-y}\text{Pr}_y\text{Ca}_{0.3}\text{MnO}_3$  for  $y = 0, 0.13, 0.4$  and  $0.5$ . The Curie temperature takes corresponding values of approximately 245, 240, 155 and 120 K. With our parameterization this corresponds, from figure 8, to  $g/W$  varying between 0.16 and 0.22. The observed variation of  $\sigma(\nu)$  with  $y$  and temperature  $T$ , over a wide range of photon energy up to  $2 \text{ eV}$ , is in general agreement with the classical treatment of Millis et al. [12]. It is possible that the unusual behaviour in the far infrared region below  $0.15 \text{ eV}$ , for  $y = 0.4$  and  $0.5$ , may relate to our calculated electronic structure in

the pseudogap in addition to direct excitation of phonons. Detailed calculations of angle-resolved photoemission and optical conductivity spectra, and their comparison with experimental data, will be reported later.

## 8 Conclusion

We have summarized the many-body CPA treatment of the double-exchange model, with and without coupling to local phonons, which is presented in detail in three earlier papers [6, 9, 7]. The method can deal with quantum local spins and phonons and is equivalent to dynamical mean field theory in the classical limit. For quite a wide range of fairly weak electron-phonon coupling we find that the results are essentially those of the pure double-exchange model. As the electron-phonon coupling is increased our theory can describe, for the first time, the crossover from the classical phonon limit [12] to the formation of small-polaron bands, and finally it links up with standard small-polaron theory in the strong-coupling limit. In section 7 we have given a much fuller discussion of the application to manganites than in the earlier papers. As well as basic properties such as Curie temperature, resistivity and magnetoresistance, we discuss the interpretation of the giant isotope effect, pressure effects and pseudogaps observed in scanning tunnelling spectroscopy, photoemission and optical conductivity.

We find that a typical manganite like  $\text{La}_{1-x}\text{Ca}_x\text{MnO}_3$ , with  $x \approx 0.33$ , is in the critical regime on the verge of small-polaron formation. This explains its extreme sensitivity to changes in parameters arising from isotopic substitution and pressure. On the other hand  $\text{La}_{1-x}\text{Sr}_x\text{MnO}_3$ , with weaker electron-phonon coupling, is quite well described by the pure double-exchange model, as pointed out by Furukawa [25]. The large pseudogap seen in a bilayer manganite [60] indicates stronger electron-phonon coupling than in most cubic manganites.

We are grateful to Lesley Cohen, D.M. Eagles, K. Kamenev, N. Furukawa and K. Kubo for helpful discussion and to the UK Engineering and Physical Sciences Research Council (EPSRC) for financial support. Elizabeth Rowley has given valuable help in preparing the manuscript for publication.

## References

- [1] A. C. Hewson, *The Kondo problem to Heavy Fermions* (Cambridge University Press, 1993).
- [2] C. Zener, Phys. Rev. **82**, 403 (1951).
- [3] P. W. Anderson and H. Hasegawa, Phys. Rev. **100**, 675 (1955).
- [4] P. G. de Gennes, Phys. Rev. **118**, 141 (1960).
- [5] K. Kubo and N. Ohata, J. Phys. Soc. Jpn. **33**, 21 (1972).
- [6] D. M. Edwards, A. C. M. Green, and K. Kubo, J. Phys.: Condens. Matter **11**, 2791 (1999).
- [7] A. C. M. Green and D. M. Edwards, J. Phys.: Condens. Matter **11**, 10511 (1999), erratum **12** 9107 (2000).
- [8] A. C. M. Green and D. M. Edwards, J. Magn. Magn. Mat. (in press).
- [9] A. C. M. Green, Phys. Rev. B **63**, 205 110 (2001).
- [10] N. Furukawa, J. Phys. Soc. Jpn. **63**, 3214 (1994).
- [11] N. Furukawa, J. Phys. Soc. Jpn. **65**, 1174 (1996).
- [12] A. J. Millis, R. Müller, and B. I. Shraiman, Phys. Rev. B **54**, 5405 (1996).
- [13] A. P. Ramirez, J. Phys.: Condens. Matter **9**, 8171 (1997).

- [14] A. J. Millis, P. B. Littlewood, and B. I. Shraiman, Phys. Rev. Lett. **74**, 5144 (1995).
- [15] J. Hubbard, Proc. Roy. Soc. **281**, 401 (1964).
- [16] R. J. Elliot, J. A. Krumhansl, and P. L. Leath, Rev. Mod. Phys. **46**, 465 (1974).
- [17] D. M. Edwards and A. C. Hewson, Rev. Mod. Phys. **40**, 810 (1968).
- [18] D. M. Edwards and J. A. Hertz, Physica B **163**, 527 (1990).
- [19] M. U. Luchini and D. M. Edwards, J. Low. Temp. Phys. **99**, 305 (1995).
- [20] M. Potthoff, T. Herrmann, and W. Nolting, Eur. Phys. J. B **4**, 485 (1998).
- [21] A. Georges, G. Kotliar, W. Krauth, and M. J. Rosenberg, Rev. Mod. Phys. **68**, 13 (1996).
- [22] R. Bulla, A. C. Hewson, and T. Pruschke, J. Phys.: Condens. Matter **10**, 8365 (1998).
- [23] R. E. Brunton and D. M. Edwards, J. Phys.: Condens. Matter **10**, 5421 (1998).
- [24] K. Kubo, J. Phys. Soc. Jpn. **36**, 32 (1974).
- [25] T. A. Kaplan and D. Mahanti, eds., *Physics of Manganites* (Kluwer Academic / Plenum Press, 1999), N Furukawa, p. 1.
- [26] T. Holstein, Ann. Phys. (N.Y.) **8**, 325 (1959).
- [27] T. Holstein, Ann. Phys. (N.Y.) **8**, 343 (1959).
- [28] H. Röder, J. Zang, and A. R. Bishop, Phys. Rev. Lett. **76**, 1356 (1996).
- [29] H. Sumi, J. Phys. Soc. Jpn. **33**, 327 (1972).
- [30] H. Sumi, J. Phys. Soc. Jpn. **36**, 770 (1974).
- [31] S. Ciuchi, F. de Pasquale, S. Fratini, and D. Feinberg, Phys. Rev. B **56**, 4494 (1997).
- [32] J. K. Freericks, M. Jarrell, and D. J. Scalapino, Phys. Rev. B **48**, 6302 (1993).
- [33] A. J. Millis, R. Müller, and B. I. Shraiman, Phys. Rev. B **54**, 5389 (1996).
- [34] G. D. Mahan, *Many-particle Physics* (Plenum Press, 1990), 2nd ed.
- [35] P. Benedetti and R. Zeyher, Phys. Rev. B **59**, 9923 (1999).
- [36] K. Held and D. Vollhardt, Phys. Rev. Lett. **84**, 5168 (2000).
- [37] D. D. S. et al. , Phys. Rev. B **53**, 6873 (1996).
- [38] W. E. Pickett and D. J. Singh, Phys. Rev. B **53**, 1146 (1996).
- [39] K. H. Kim, J. Y. Gu, H. S. Choi, G. W. Park, and T. W. Noh, Phys. Rev. Lett. **77**, 1877 (1996).
- [40] A. Urushibara, Y. Moritomo, T. Arima, A. Asamitsu, G. Kido, and Y. Tokura, Phys. Rev. B **51**, 14103 (1995).
- [41] D. N. McIlroy, C. Waldfried, J. Zhang, J.-W. Choi, F. Foong, S. H. Liou, and P. A. Dowben, Phys. Rev. B **54**, 17438 (1996).
- [42] M. C. Martin, G. Shirane, Y. Endoh, K. Hirota, Y. Moritomo, and Y. Tokura, Phys. Rev. B **53**, 14285 (1996).

- [43] P. Dai, J. Zhang, H. A. Mook, S.-H. Liou, P. A. Dowben, and E. W. Plummer, *Phys. Rev. B* **54**, R3694 (1996).
- [44] D. Louca, T. Egami, E. L. Brosha, H. Röder, and A. R. Bishop, *Phys. Rev. B* **56**, R8475 (1997).
- [45] A. Moreo, S. Yunoki, and E. Dagotto, *Science* **283**, 2034 (1999).
- [46] M. Mayr, A. Moreo, J. A. Vergés, J. Arispe, A. Feiguin, and E. Dagotto, *condmat/0007480* (2000).
- [47] E. L. Nagaev, *Phys. Lett. A* **258**, 65 (1999).
- [48] A. S. Alexandrov and A. M. Bratovsky, *Phys. Rev. Lett.* **82**, 141 (1999).
- [49] A. S. Alexandrov and A. M. Bratovsky, *J. Phys.: Condens. Matter* **11**, 1989 (1999).
- [50] Comment and reply on ref. [48], *Phys. Rev. Lett.* **84**, 2042 (2000).
- [51] A. S. Alexandrov and A. M. Bratovsky, *J. Phys.: Condens. Matter* **11**, L531 (1999).
- [52] D. M. Eagles, *Phys. Rev.* **145**, 645 (1966).
- [53] G. M. Zhao, D. J. Kang, W. Prellier, M. Rajeswari, H. Keller, T. Venkatesan, and R. L. Greene, *Phys. Rev. B* **62**, R11949 (2000).
- [54] E. L. Nagaev, *Phys. Rev. B* **58**, 12242 (1998).
- [55] J. P. Franck, I. Isaac, W. Chen, J. Chrzanowski, and J. C. Irwin, *Phys. Rev. B* **58**, 5189 (1998).
- [56] G. M. Zhao, K. Conder, H. Keller, and K. A. Müller, *Nature* **381**, 676 (1996).
- [57] J. J. Neumeier, M. F. Hundley, J. D. Thompson, and R. H. Heffner, *Phys. Rev. B* **52**, R7006 (1995).
- [58] J. Y. T. Wei, N.-C. Yeh, and R. P. Vasquez, *Phys. Rev. Lett.* **79**, 5150 (1997).
- [59] A. Biswas, S. Elizabeth, A. K. Raychaudhuri, and H. L. Bhat, *Phys. Rev. B* **59**, 5368 (1999).
- [60] D. S. Dessau, T. Saitoh, C.-H. Park, Z.-X. Shen, P. Villeda, N. Hamada, Y. Moritomo, and Y. Tokura, *Phys. Rev. Lett.* **81**, 192 (1998).
- [61] A. Moreo, Y. S, and E. Dagotto, *Phys. Rev. Lett.* **83**, 2773 (1999).
- [62] K. H. Kim, J. H. Jung, D. J. Eom, T. W. Noh, J. Yu, and E. J. Choi, *Phys. Rev. Lett.* **81**, 4983 (1998).